

Interactive comment on “Chemical characteristics and causes of airborne particulate pollution in warm seasons in Wuhan, central China” by X. P. Lyu et al.

Anonymous Referee #3

The manuscript by Lyu et al. offers interesting results on the chemical compositions of PM and precursors in Wuhan China, in specific campaigns in 2014. In my opinion, results are noteworthy but several revisions are necessary before publication in ACP.

Reply: We thank the reviewer for his/her positive and encouraging comments. Detailed responses to the specific comments were listed point by point below.

1. Abstract needs significant improvement. It should be self-explanatory. For examples cases explanation is missing. K is 47% of what? etc.

Reply: Thanks for the suggestion. The abstract was substantially revised, including the points raised by the reviewer.

For details, please refer to lines 15-33.

2. Introduction. The first sentence is not needed.

Reply: Accepted with thanks. In addition, we also revised the second sentence as follows.

Airborne particulate pollution, also called “haze,” has swept across China in recent years, particularly over its northern, central, and eastern parts (Cheng et al., 2014; Kang et al., 2013; Wang et al., 2013).

For details, please refer to lines 37-39.

3. English should be significantly improved. Some sentences are too simple for a scientific journal. Some terms need corrections (ammonia in page 2; the use of past tense should be avoided for general sentences like EC was the typical tracer of uncomplete combustion; aromatically instead of automatically etc....). Syntaxis also needs improvement.

Reply: Thanks for pointing out the errors. The grammatical errors and typos pointed out by the reviewer were corrected. To thoroughly improve the quality of the manuscript, we have asked an editing company to correct grammars and syntaxes before the submission of the revised version.

4. I advice the use of SIA instead of SIOA.

Reply: Accepted with thanks. Replacements were made throughout the whole manuscript.

5. Do authors mean wildfires with the term "fire spot"?

Reply: Exactly. The use of “fire spot” was replaced with “wildfires” throughout the whole manuscript.

6. Information on traffic volume next to the monitoring site is lacking.

Reply: Thanks for the useful comment. More details about the sampling site including traffic volume were provided as follows.

The traffic volume of the road was around 200 vehicles per hour. However, a wall (~2 m high) and several rows of trees (7 to 8 m high) were located between the road and the sampling site.

For details, please refer to lines 123-125.

7. The TEOM model does not include FDMS. Authors should discuss what uncertainty does this add to the conclusions.

Reply: Thanks for the comments. In this study, a filter dynamics measurement system (FDMS) was integrated into the TEOM system to correct the measurement deviation of the TEOM system caused by mass loss of semi-volatile particulate matters. Revisions were made as follows:

PM₁₀ and PM_{2.5} were measured with a continuous ambient particulate monitor (Thermo Fisher-1405D, USA) integrated with a filter dynamics measurement system to minimize the loss of semivolatile particulate matter.

For details, please refer to lines 126-128.

8. Rephrase sentence in rows 199-200 and 223-224.

Reply: Accepted with thanks. The sentences were rephrased as follows.

Bearing in mind that the sampling site, period, method, and instrument all interfere with comparisons, the ambient particulate pollution in Wuhan was severe.

For details, please refer to lines 222-224.

Because smaller particles tend to pose more harm to human health and to the atmosphere due to their larger specific surface areas (Yang et al., 2012; Goldberg et al., 2001), and because the chemical compositions in PM_{10} were not analyzed, this study focused mainly on $PM_{2.5}$.

For details, please refer to lines 243-245.

9. What do you mean with "completely" in row 225?

Reply: Thanks for pointing out the inappropriate use of “completely”. Since this sentence was rewritten, this word was not used. Please refer to lines 243-245 for details.

10. Row 233: not fully true, also primary OC and EC are fine particles.

Reply: Thanks for the valuable comments. We fully agreed to the reviewer that primary OC and EC also constitute fine particles. The discussion in this part was revised as follows.

The $PM_{2.5}/PM_{10}$ value also increased remarkably on episode days compared to that on non-episode days, except for episode 2 ($45.9\% \pm 2.5\%$), which suggests that more secondary species and/or primary fine particles (e.g., primary OC and EC generated from combustion) were generated or released during the episodes. In contrast, the lower $PM_{2.5}/PM_{10}$ value during episode 2 might imply a strong source of coarse particles. Indeed, this inference was confirmed by the source apportionment analysis in section 3.3.3.

For details, please refer to lines 253-258.

11. I would rather use the term episode instead of case.

Reply: Accepted with thanks. Changes were made throughout the whole manuscript.

12. Row 240: the contribution of fugitive dust is estimated in $5 \mu\text{g}/\text{m}^3$, well before the Source apportionment section. Please reorder.

Reply: Thanks for the suggestion. The sentences were revised as follows.

In contrast, the lower $PM_{2.5}/PM_{10}$ value during episode 2 might imply a strong source of coarse particles. Indeed, this inference was confirmed by the source apportionment analysis in section 3.3.3.

For details, please refer to lines 256-258.

13. Relating sulfate to point source and nitrate to mobile ones, is too simplistic. Traffic also emit primary particles, and no₃ can also come from industries.

Reply: The comment is highly appreciated. We fully agree with the reviewer. Since this short discussion was not closely related to the aims of this manuscript, it was removed.

14. How OC_{non-comb} was estimated?? the reference Cabada et al., 2004 is missing in the Bibliography. More clarification is needed here. Do they mean that biogenic OC is all primary??

Reply: Thanks for the question. OC_{non-comb} means primary OC that is not related to combustion. As the intercept in the regression (Figure 5), OC_{non-comb} did not vary with EC (the independent variable) which was primarily emitted from combustion activities. OC_{non-comb} might include primary biogenic OC, however it did not mean that biogenic OC is all primary. In fact, this method has been extensively used to estimate POC and SOC (*e.g.*, Chu et al., 2005; Saylor et al., 2006). The method to estimate OC_{non-comb} was further clarified, and revisions were made in the manuscript.

where $(OC/EC)_{prim}$ was the ratio of primary OC to EC, obtained from the pairs of OC and EC with the OC/EC ratios among the 10% lowest; and OC_{non-comb} was the primary OC that was not related to combustion activities. These values were determined by the slope and intercept of the linear regression between primary OC and EC, respectively (Figure 5).

For details, please refer to lines 305-308.

The missing reference was added. For details, please refer to lines 603-605.

15. Row 295: p value is missing.

Reply: Sorry for the carelessness. " $p < 0.05$ " was added.

For detail, please refer to line 313.

16. Row 280: provide references for value of 2.

Reply: Accepted with thanks.

For details, please refer to line 298.

17. Figure 6: how authors interpret daily variation of HO₂.

Reply: Excellent question. The diurnal variation of HO₂ presents bimodal – one at daytime hours and another at night. The daytime pattern of HO₂ is typically bell-shaped peaked at noon or in early afternoon, consistent with the variation of atmospheric oxidative capacity (*i.e.*, O₃ generally peaks at noon or in early afternoon). Solar radiation is the main driving factor of this pattern. Namely, when the radiation is the strongest at noon, the photochemical reactions are the most intensive, which results in the highest production of O₃ and oxidative radicals including HO₂. Another peak of HO₂ is usually observed in the evening because reactions among alkenes and O₃ and NO₃ lead to the formation of HO₂. Since concentrations of alkenes increase rapidly from late afternoon to the evening due to the decreasing photochemical consumption, increasing emissions from vehicles at rush hours in the evening, and reduction of boundary layer, the HO₂ production subsequently increases. With the consumption of O₃ and NO₃, the reactions with alkenes weaken in late evening. In addition, reactions among radicals consume HO₂. Hence, HO₂ decreases from late evening to early morning.

Overall, the mechanisms of HO₂ production and loss are complicated, and it is difficult to comprehensively discuss them in this paper. Therefore, we briefly explained the diurnal pattern of HO₂ in the revised manuscript.

Two peaks were found for the simulated diurnal pattern of HO₂, which might be caused by strong solar radiation at noon and in the early afternoon and by reactions among alkenes and O₃ and NO₃ at night (Emmerson et al., 2005; Kanaya et al., 1999).

For details, please refer to lines 318-320.

18. Section 3.2.2. there is a contrast between the conclusion that all PM components increase during episodes (row 324) and that the OC decreases (row 329).

Reply: Sorry for the confusion. The results are not contradictory because the absolute concentrations of PM_{2.5} components increased while the fraction (percentage) of OC in PM_{2.5} decreased during the episodes.

To avoid confusion, both concentration and percentage were provided in Table 3 in the revised manuscript. Subsequently, the discussion was revised as follows.

Table 3 summarizes the mass concentrations and percentages of the main components in PM_{2.5}. The mass concentrations of PM_{2.5} components significantly increased from non-episode days to episode days ($p < 0.05$). In contrast, the percentages of the chemical components in PM_{2.5} varied by species. In summer, the fractions of EC and K in PM_{2.5} experienced significant increases from non-episode 1 (EC, 4.8% \pm 0.2%; K, 2.0% \pm 0.1%) to episode 1 (EC, 5.7% \pm 0.5%; K, 4.4% \pm 0.3%) and episode 3 (EC, 5.3% \pm 0.2%; K, 3.0% \pm 0.2%). Because EC is the tracer of incomplete combustion (Chow et al., 1996) and K is the indicator of biomass burning (Saarikoski et al., 2007; Echalar et al., 1995), the higher percentages of EC and K in episodes 1 and 3 imply the outstanding contribution of biomass burning. In contrast, the fraction of OC in PM_{2.5} remained stable on both episode and non-episode days ($p > 0.05$), possibly because the high temperatures in summer hindered the gas-to-particle partitioning of semivolatile organics (Takekawa et al., 2003). Furthermore, the percentages of Ca (2.9% \pm 0.4%) and Fe (2.7% \pm 0.3%) significantly increased during episode 2 ($p < 0.05$) compared to those in non-episode 1 (Ca, 1.1% \pm 0.1%; Fe, 1.5% \pm 0.1%), which shows that fugitive dust made a considerable contribution to PM_{2.5} in episode 2. In addition, biomass burning might also have contributed to PM_{2.5}, in view of the increase in the percentage of K (non-episode 1, 2.0% \pm 0.1%; episode 2, 3.2% \pm 0.2%).

In autumn, the percentage of K significantly ($p < 0.05$) increased during episode 4 (3.1% \pm 0.1% vs. 2.1% \pm 0.1% in non-episode 2), as did that of OC (27.3% \pm 0.7% vs. 20.9% \pm 0.8% in non-episode 2), suggesting the dominant role of biomass burning in episode 4. Furthermore, the fractions of OC in episode 5 (23.8% \pm 1.5%) and NO₃⁻ in episode 6 (26.1% \pm 1.0%) were obviously higher than those in non-episode 2 (OC, 20.9% \pm 0.8%; NO₃⁻, 19.8% \pm 0.9%). Due to the complexity of the sources of OC and NO₃⁻, the causes of episodes 5 and 6 are further explored in the following sections.

In summary, episodes 1, 3, and 4 were greatly affected by biomass burning. This finding was further confirmed by the significant increases in the gaseous tracers of biomass burning such as ethyne (C₂H₂) and methyl chloride (CH₃Cl) (Guo et al., 2011b; Simoneit et al., 2002) during these episodes ($p < 0.05$; see Figure S8 in the Supplement).

As this part was more related to the causes of PM_{2.5} episodes, it was moved to section 3.3.2 “Chemical signatures” under section 3.3 “Causes of PM_{2.5} episodes”. For details, please refer to lines 378-404, Table 3 and Figure S8 in the supplement.

19. If cases 1 and 3 are attributed to Biomass burning, why OC decreases? BB is the largest source of OC, as shown in Figures 10 and 11.

Reply: Thanks for the question. As explained above, the absolute concentration of OC increased remarkably in episodes 1 and 3, while the percentage of OC in PM_{2.5} decreased. Since the decrease in percentage was not significant ($p > 0.05$), we revised the wording to “the fraction of OC in PM_{2.5} remained stable”. Furthermore, the possible reason for the stable percentage of OC was given.

In contrast, the fraction of OC in PM_{2.5} remained stable on both episode and non-episode days ($p > 0.05$), possibly because the high temperatures in summer hindered the gas-to-particle partitioning of semivolatile organics (Takekawa et al., 2003).

For details, please refer to lines 386-389.

20. Ca and Fe also come from traffic and construction/demolition works. And K in case 2 can also be emitted by mineral sources.

Reply: We agreed with the reviewer. In this study, fugitive dust included dust from traffic, construction/demolition works, yard and bare soil. The following was added into the revised manuscript:

Because Fe and Ca are typical crustal elements, fugitive dust (e.g., dust from traffic, construction and demolition works, yards, and bare soil) was their most likely source.

For details, please refer to lines 342-343.

In addition, correlation analyses among the main elements were carried out. Weak correlations of K with Fe and Ca were found. Thus, the possibility of K emitted from mineral source was eliminated in this study. The following was added into the revised manuscript.

Correlation analysis indicated that Fe had good correlation with Ca ($R^2 = 0.66$; Figure S7 in the Supplement), whereas weak correlations of K with Fe ($R^2 = 0.14$) and Ca ($R^2 = 0.09$) were found, suggesting that Fe and Ca shared common sources that were different from the sources of K. Because Fe and Ca are typical crustal elements, fugitive dust (e.g., dust from traffic, construction and demolition works, yards, and bare soil) was their most likely source. In contrast, apart from emissions from mineral sources, K is also emitted from biomass burning. As such, K was

believed to be mainly emitted from biomass burning in this study, which is further supported by the moderate correlations of K with OC ($R^2 = 0.52$) and EC ($R^2 = 0.48$) because biomass burning also emits OC and EC (Saarikoski et al., 2007; Echalar et al., 1995).

For details, please refer to lines 338-347.

21. The source apportionment section lacks of many details which are needed to ensure that the solution is the more realistic one. Why authors decide to perform separate PMFs for different cases? They at least present also the total (assembled) PMF, which will certainly improve statistically significance and reduce random and rotational errors of the solution.

Reply: The excellent comments are highly appreciated. The source apportionment part was revised substantially according to the reviewer's suggestions. The revisions included:

(1) Source apportionment was performed together with all case data collected in both episodes and non-episodes. However, since summer data of water soluble ions (WSIs) were not available, the source apportionments in summer (including episodes 1, 2, 3 and non-episode 1) and autumn (including episodes 4, 5, 6 and non-episode 2) were still separately conducted.

For details, please refer to section 3.3.3 "source apportionment".

(2) The selection criteria for best solution and the evidences (Q value, residual, G-space plot and etc.) were provided.

The selection of the factor number and the best solution depended upon the following criteria. (1) A lower Q value (Equation 6; a function to evaluate the model runs) was preferable. (2) The ratio between Q_{robust} and Q_{true} was lower than 1.5. In this study, the ratios were 0.8 and 0.9 for the summer and autumn data simulation, respectively. (3) Good agreement was shown between the predicted and observed $PM_{2.5}$. The slope and correlation coefficient (R^2) for the linear regression were 0.91 and 0.86 in summer and 0.95 and 0.98 in autumn, respectively, as shown in Figure S2 in the Supplement. The lower R^2 value seen during the summer might be due to the lack of WSI data. (4) The residuals were normally distributed between -3 and 3 . Table S2 summarizes the percentage of samples with residuals between -3 and 3 for each species; the lowest percentages were 92.9% and 96.0% for Ni in summer and autumn, respectively. The scaled residuals for $PM_{2.5}$ are shown in Figure S3 in the Supplement. The percentage of residuals between -3 and 3

was comparable between summer (97.5%) and autumn (98.1%). Finally (5), no correlation was found between the factors, which was achieved by examining the G-space plots and controlled by the FPEAK model runs. Figures S4 and S5 in the Supplement present the G-space plots in summer and autumn, respectively. The low factor contributions and poor correlations indicated that rotational ambiguity was effectively controlled.

For details, please refer to lines 189-204.

22. The lack of SIA in summer is a critical issue. They are a major contributor to the mass, so the PM source apportionment has certainly larger errors than in autumn. This needs to be discussed, showing residuals of PM and performing error estimate tools, such as BS, DISP and BS-DISP which are implemented in EPA PMFv5.

Reply: Many thanks for the excellent comment. The scaled residuals of PM_{2.5} are provided in Figure S3 in the Supplement. It was found that the residuals were normally distributed between -3 and 3. However, the percentage of samples with residuals between -3 and 3 was comparable between summer (97.5%) and autumn (98.1%). In addition, bootstrap method was used to estimate the errors. According to the standard deviations estimated by bootstrap, we calculated 95% confidence intervals, which are shown as error bars in Figures 10 and 11. The error was even smaller in summer (0.6 µg/m³; 0.7%) than that in autumn (2.6 µg/m³; 3.2%).

The agreement between the predicted and observed PM_{2.5} was also used to evaluate the simulation, as presented in Figure S2. The agreement was indeed lower in summer (slope=0.91; R²=0.86) than that in autumn (slope=0.95; R²=0.98). Relevant discussion was provided as follows.

(3) Good agreement was shown between the predicted and observed PM_{2.5}. The slope and correlation coefficient (R²) for the linear regression were 0.91 and 0.86 in summer and 0.95 and 0.98 in autumn, respectively, as shown in Figure S2 in the Supplement. The lower R² value seen during the summer might be due to the lack of WSI data. (4) The residuals were normally distributed between -3 and 3. Table S2 summarizes the percentage of samples with residuals between -3 and 3 for each species; the lowest percentages were 92.9% and 96.0% for Ni in summer and autumn, respectively. The scaled residuals for PM_{2.5} are shown in Figure S3 in the

Supplement. The percentage of residuals between -3 and 3 was comparable between summer (97.5%) and autumn (98.1%).

For details, please refer to lines 192-200, Table S2, Figure S2 and Figure S3 in the Supplement.

A bootstrap method was used to estimate the model errors, according to which 95% confidence intervals (CIs) were calculated. The 95% CI for PM_{2.5} was 0.6 µg/m³ (0.7% of predicted PM_{2.5}) in summer and 2.6 µg/m³ (3.2% of predicted PM_{2.5}) in autumn.

For details, please refer to lines 205-207.

23. By the way which software have been used? What uncertainty of the data have been used as input? Was the Q -values the only criterion used for number of factor selection? What about distribution of residuals, G space plot, factor profiles in g/g (which are missing and need to be shown)....?

Reply: Thanks a lot for the questions about the PMF model. In this study, EPA PMF v5.0 was used to conduct the source apportionment analysis. The uncertainties were set as follows.

The uncertainties were $\sqrt{(10\% \times \text{concentration})^2 + \text{DL}^2}$ and $5/6 \times \text{DL}$ for the samples with concentrations higher and lower than DL, respectively.

For details, please refer to line 175 and lines 185-186.

The criteria used for the selection of factor number and the best solution were provided in the answer to comment 21, which involved Q-value, the ratio between Q_{robust} and Q_{true}, agreement between the predicted and observed values, residuals and G-space plot. The factor profiles are provided in Figures 10 and 11 in the revised manuscript.

For details, please refer to lines 189-204 and Figures 10 and 11.

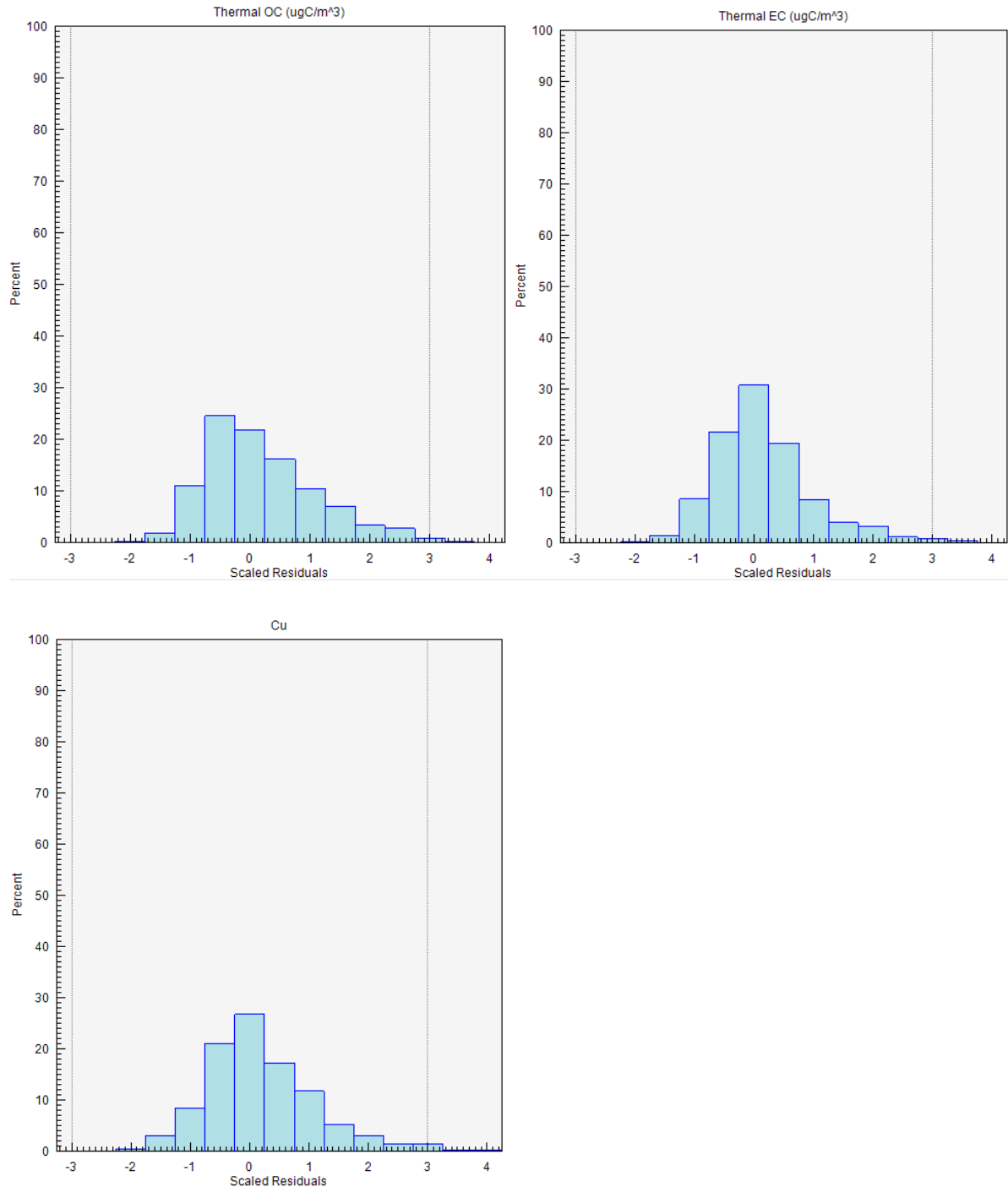
24. Traffic is missing among the sources. This is hard to believe for a mega city. There must be a mix of sources, so that solutions with 5, 6...factors should be explored. Residuals of OC, EC, Cu should be provided.

Reply: Thank you very much for the great comments and suggestions. In the revised manuscript, 5 and 6 sources including traffic emissions were identified in summer and autumn, respectively.

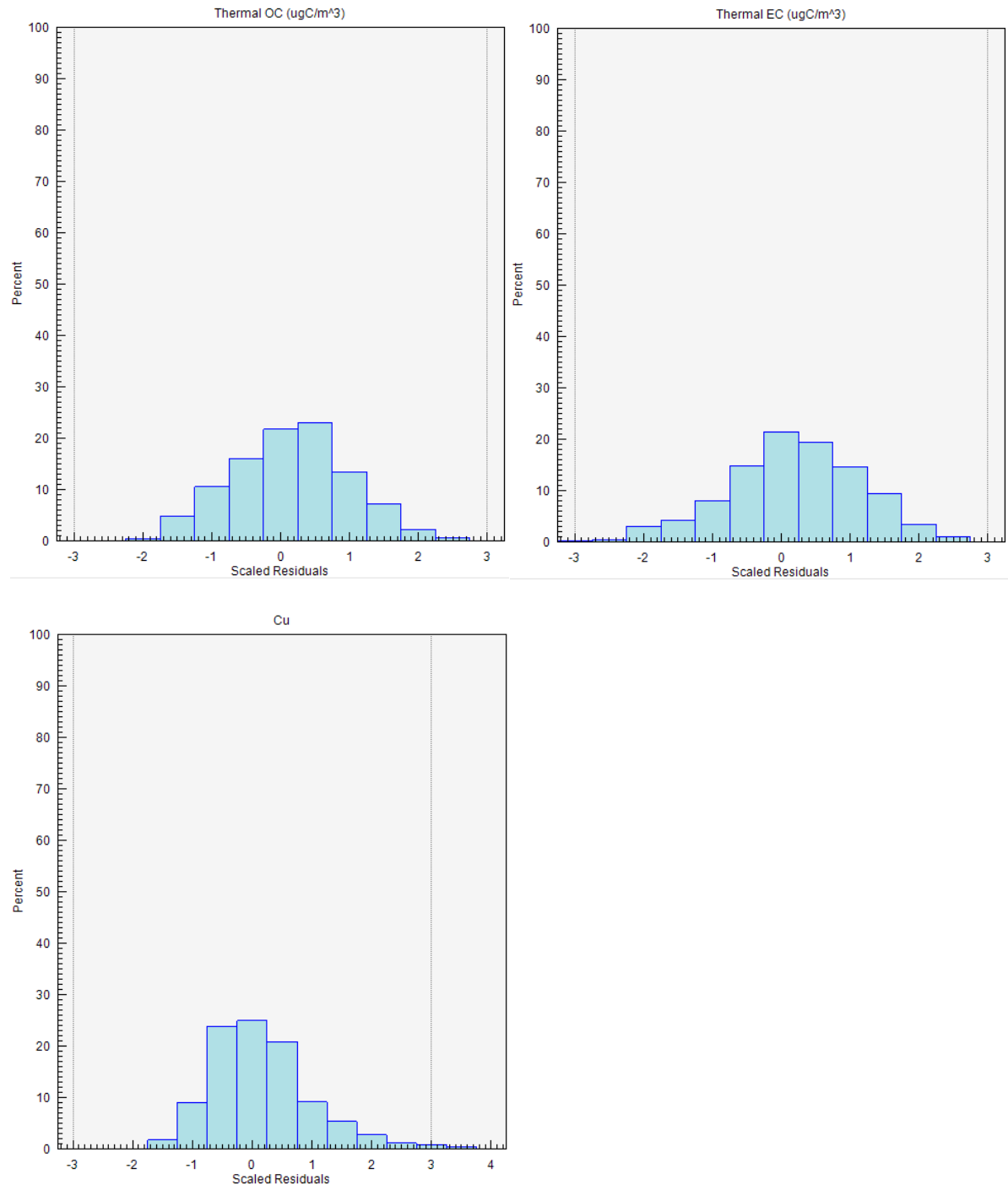
Table S2 in the supplement lists the percentage of samples with residuals between -3 and 3. Also, the residuals of OC, EC and Cu were provided here for the reviewer's reference.

For details, please refer to section 3.3.3 "Source apportionment".

Residuals of OC, EC and Cu in summer:



Residuals of OC, EC and Cu in autumn:



25. Back trajectories are presented, but please specify which day did you select for each case? Cases span over several days... and the selection should be supported by some discussion.

Reply: Thanks for the suggestion. Yes, the backward trajectories were simulated during the entire period of each episode. The reason for this selection was also provided as follows.

Because the concentrations, compositions and source contributions of $PM_{2.5}$ were averaged over the entire period of each episode, the wildfire distribution and backward trajectories were also averaged for the entire period of each episode.

For details, please refer to lines 434-437.

26. Row 546 "between" should be replaced by "with".

Reply: Thanks for the correction. Replaced as suggested.

For details, please refer to line 519.

27. The conclusion in row 608, should be revisited. The lack of SIA data in summer does not allow to draw comprehensive knowledge of $PM_{2.5}$.

Reply: Thanks for the suggestion. This sentence was revised as follows.

This study **advances our understanding of the** chemical characteristics of $PM_{2.5}$ in warm seasons in Wuhan and for the first time quantifies the contribution of biomass burning to $PM_{2.5}$.

For details, please refer to lines 581-582.

References:

Chu, S.H., 2005. Stable estimate of primary OC/EC ratios in the EC tracer method. *Atmos. Environ.* 39(8), 1383-1392.

Saylor, R.D., Edgerton, E.S., and Hartsell, B.E., 2006. Linear regression techniques for use in the EC tracer method of secondary organic aerosol estimation. *Atmos. Environ.* 40(39), 7546-7556.

Anonymous Referee #4

The paper on chemical composition and source analysis by Lyu et al. presents interesting results for Wuhan, China and would be a good addition to the literature on the topic. The paper discusses chemical composition of PM_{2.5}, possible sources and formation mechanisms for SIA and SOA. However, I have a few questions and suggestions for the authors before the paper is accepted for publication. Some of the sections of the paper present conflicting information, and the introduction section needs to be thoroughly edited (e.g. Lines 39-40, 46, 51-52, 60-62).

Reply: The great comments and suggestions are highly appreciated, which helped us to improve the manuscript substantially. The introduction section was revised according to the reviewer's comments. In addition, the grammatical errors and typos in the manuscript were corrected by an editing company before the revised manuscript was submitted. Detailed responses to the specific comments were provided point by point below.

Airborne particulate pollution, also called "haze," has swept across China in recent years, particularly over its northern, central, and eastern parts (Cheng et al., 2014; Kang et al., 2013; Wang et al., 2013).

Numerous studies have been conducted in China to understand the spatiotemporal variations in particle concentrations, the chemical compositions, and the causes of haze events (Cheng et al., 2014; Cao et al., 2012; Zheng et al., 2005; Yao et al., 2002).

For details, please refer to lines 37-39 and lines 48-50.

Specific Comments:

1. Lines 204-205: Please clarify- ". . . related to variations in number of construction sites.. " Is there a considerable variation in the number of active construction sites? It is surprising that the contribution from carbonaceous aerosols to total PM is very low. It is somewhat counterintuitive that OC did not increase during the pollution episodes (Lines 328-338), since the increase is being attributed to biomass burning. In autumn, however, an increase in OC is associated with biomass burning. This is not coherent.

Reply: Thank you very much for the excellent comments. Since it is difficult to get the exact number of construction sites, we explained the variations of PM₁₀ as follows.

From summer to autumn, PM₁₀ levels declined considerably from 135.1 ± 4.4 to 118.9 ± 3.7 $\mu\text{g}/\text{m}^3$, whereas PM_{2.5} remained statistically stable ($p > 0.05$). The higher summer PM₁₀ concentration was probably related to a higher load of fugitive dust. In Wuhan, the temperature ($25.6 \text{ }^\circ\text{C} \pm 0.2 \text{ }^\circ\text{C}$) in summer was considerably higher than that ($17.5 \text{ }^\circ\text{C} \pm 0.3 \text{ }^\circ\text{C}$) in autumn ($p < 0.05$), which led to lower water content in the soil and a higher tendency of dust suspension. In addition, the average wind speed in summer (1.2 ± 0.04 vs. 0.8 ± 0.03 m/s in autumn) was also higher ($p < 0.05$), which could also have favored the generation of fugitive dust.

For details, please refer to lines 225-231.

In this study, carbonaceous aerosols constituted $23.2 \pm 0.5\%$ of PM_{2.5}, which was comparable to those (17.7% at an urban site and 17.8% at a suburban site) reported by Zhang et al. (2015) in Wuhan.

For the variations of OC, we are sorry for the confusion about absolute concentration and percentage. In this study, the absolute concentrations of OC and EC greatly increased in all the episodes. However, the percentage (or fraction) of OC in PM_{2.5} remained stable in episode 1 and episode 3 compared to non-episode 1, while the percentage of OC increased in all episodes in autumn compared to non-episode 2. This discrepancy might be due to the fact that high temperature suppressed the gas-to-particle partitioning of semi-volatile organics in summer. To avoid confusion, the concentrations and percentages of main PM_{2.5} components including OC were provided in Table 3 in the revised manuscript. And the explanation for the stable percentage of OC in summer episodes was provided as follows.

In contrast, the fraction of OC in PM_{2.5} remained stable on both episode and non-episode days ($p > 0.05$), possibly because the high temperatures in summer hindered the gas-to-particle partitioning of semivolatile organics (Takekawa et al., 2003).

For details, please refer to lines 386-389 of section 3.3.2 “Chemical signatures” and Table 3.

2. Lines 268-273: This estimation can help interpret if the ions are neutralized. Consider expanding this section to include a discussion on whether or not the aerosols were neutralized during autumn season.

Reply: Accepted with thanks. The discussion was supplemented as follows.

When extending NH_4^+ to total cations (NH_4^+ , Ca^{2+} , Mg^{2+} , Na^+ , and K^+) and NO_3^- and SO_4^{2-} to total anions (NO_3^- , SO_4^{2-} , and Cl^-), the molar charges of the cations and anions were balanced (slope, 0.98; $R^2 = 0.98$), as shown in Figure S6 in the Supplement, indicating that $\text{PM}_{2.5}$ was neutralized during autumn in Wuhan.

For details, please refer to lines 288-291 and Figure S6.

3. Were the correlations between different metals analysed? Some of the K can also come from sources other than biomass burning (especially crustal material), and it would be useful to understand if that is the case. This is particularly relevant with reference to the earlier comment about construction sites. Also, was K found to be correlated with OC/EC?

Reply: Excellent comments. The correlation analyses were supplemented in the revised manuscript as follows.

Correlation analysis indicated that Fe had good correlation with Ca ($R^2 = 0.66$; Figure S7 in the Supplement), whereas weak correlations of K with Fe ($R^2 = 0.14$) and Ca ($R^2 = 0.09$) were found, suggesting that Fe and Ca shared common sources that were different from the sources of K. Because Fe and Ca are typical crustal elements, fugitive dust (e.g., dust from traffic, construction and demolition works, yards, and bare soil) was their most likely source. In contrast, apart from emissions from mineral sources, K is also emitted from biomass burning. As such, K was believed to be mainly emitted from biomass burning in this study, which is further supported by the moderate correlations of K with OC ($R^2 = 0.52$) and EC ($R^2 = 0.48$) because biomass burning also emits OC and EC (Saarikoski et al., 2007; Echalar et al., 1995).

For details, please refer to lines 338-347.

4. PMF: The authors do not provide any details about the outputs, and the process used for determining the factor number, or the stability of the factors. How was the uncertainty estimated? In the current analysis, the fourth factor (biomass burning) seems to include SIA, SOA and the typical biomass burning tracers. Is it possible to tease out secondary aerosol factors if 5-7 factor solutions are used? What was the total sample size used for PMF analysis? Is traffic not a source for PM in the sampling region?

Reply: Many thanks for the great comments. The same comments are also given by another reviewer. In the revised manuscript, new source apportionment simulations were performed, which separated the source of SIA and traffic. Details about the PMF outputs were also provided. Source profiles are shown in Figures 10 and 11. Source contributions are listed in Table 4. Besides, section 2.3 provided other details about the PMF inputs and outputs, *i.e.*, estimates of uncertainties, sample sizes, Q values, agreement between the predicted and observed values, the residuals and G-space plots. The model errors were estimated with the bootstrap method in PMF. For details, please refer to lines 183-204, Figures 10 and 11, Table 4 and section 3.3.3 “Source apportionment”.

Technical comments.

5. Please proofread the manuscript carefully, and edit for language. Line 24: Contribution for PM10 or PM2.5?

Reply: Thanks for the suggestion. To ensure the quality of the manuscript, the grammatical errors and typos in this manuscript were corrected by an editing company before the revised manuscript was submitted.

The contribution of $47.0 \pm 2.2\%$ was related to the total metal elements in PM_{2.5}. Since the abstract was substantially revised, the wording did not exist in the revised manuscript.

6. Methods: Were these hourly measurements? Which method was used for OC/EC analysis? Please include 1-2 lines about the custom element analyser.

Reply: Thanks for the questions and suggestion. Yes, PM and the chemical compositions were all hourly measurements. NIOSH thermal-optical transmission (TOT) method was used for OC/EC analysis. More detailed introduction about the customized metal analyzer was provided.

Hourly data were obtained for each species.

... and an aerosol OC/EC online analyzer (Sunset-RT-4, USA); the NIOSH thermal-optical transmission method was used to resolve the carbonaceous aerosols (OC and EC).

This instrument used a PM_{2.5} impactor to collect the airborne particulate samples, which were analyzed by the β-ray in terms of mass concentrations. The filters loaded with particles were then sent to an x-ray fluorescence analysis system for quantitative analysis.

For details, please refer to lines 118-119, lines 130-132 and lines 133-135.

7. Table 1: For some cities (e.g. Beijing), is the reported value the arithmetic mean, or some other statistic? Please clarify. Also, change Tai Wan to Taiwan.

Reply: Thanks for the question and suggestion. Yes, the values cited from Liu et al. (2014) (Beijing) and Deng et al. (2015) (Guangzhou) were arithmetic means, which were specified in the revised manuscript. Tai Wan was revised to Taiwan.

For details, please refer to Table 1 and line 235.

8. Lines 60-62: Please rephrase.

Reply: Accepted with thanks. The sentence was rephrased as “In general, secondary species and mineral or sea salt components are prone to be apportioned in fine and coarse particles (Zhang et al., 2013; Theodosi et al., 2011)”.

For details, please refer to lines 57-58.

9. Lines 194-195: Either specify when these statistical parameters are reported in Table 1, or remove this sentence.

Reply: Thanks for the suggestion. The statistical values in Table 1 were specified.

For details, please refer to Table 1 and line 235.

10. Lines 202-207: How strong was the correlation between the two fractions of PM? Was there a difference in this relationship during the episode compared to non-episode days?

Reply: Thanks for the great questions. Overall, PM_{2.5} had fair correlation with PM₁₀ ($R^2=0.59$). The correlation was better in autumn ($R^2=0.70$) than that in summer ($R^2=0.54$). In addition, their correlation (PM_{2.5} vs. PM₁₀) was comparable between episodes ($R^2=0.44$) and non-episodes ($R^2=0.42$). However, all these correlations cannot explain why PM₁₀ decreased in autumn while PM_{2.5} remained stable. Combining your first specific comment, we revised this paragraph as follows.

From summer to autumn, PM₁₀ levels declined considerably from 135.1 ± 4.4 to 118.9 ± 3.7 $\mu\text{g}/\text{m}^3$, whereas PM_{2.5} remained statistically stable ($p > 0.05$). The higher summer PM₁₀ concentration was probably related to a higher load of fugitive dust. In Wuhan, the temperature ($25.6 \text{ }^\circ\text{C} \pm 0.2 \text{ }^\circ\text{C}$) in summer was considerably higher than that ($17.5 \text{ }^\circ\text{C} \pm 0.3 \text{ }^\circ\text{C}$) in autumn ($p < 0.05$), which led to lower water content in the soil and a higher tendency of dust suspension. In addition, the average wind speed in summer (1.2 ± 0.04 vs. 0.8 ± 0.03 m/s in autumn) was also higher ($p < 0.05$), which could also have favored the generation of fugitive dust.

For details, please refer to lines 225-231.

11. Lines 223-224: What does this sentence mean- “. . . Due to the fact that the chemical, optical and toxic properties tend to be more apparent in smaller particles..”

Reply: Sorry for the confusion. This sentence was rephrased as follows.

Because smaller particles tend to pose more harm to human health and to the atmosphere due to their larger specific surface areas (Yang et al., 2012; Goldberg et al., 2001), and because the chemical compositions in PM₁₀ were not analyzed, this study focused mainly on PM_{2.5}.

For details, please refer to lines 243-245.

12. Lines 233-234: PM_{2.5} isn't entirely composed of secondary particles. Please edit the statement.

Reply: Thanks for the excellent comment. The statement “PM_{2.5}/PM₁₀ was a measure of the proportion of secondary species in particles.” was deleted. Instead, the discussion was revised as follows.

The PM_{2.5}/PM₁₀ value also increased remarkably on episode days compared to that on non-episode days, except for episode 2 ($45.9\% \pm 2.5\%$), which suggests that more secondary species and/or primary fine particles (e.g., primary OC and EC generated from combustion) were generated or released during the episodes. In contrast, the lower PM_{2.5}/PM₁₀ value during episode 2 might imply a strong source of coarse particles. Indeed, this inference was confirmed by the source apportionment analysis in section 3.3.3.

For details, please refer to lines 253-258.

13. Line 295: p-value is missing.

Reply: Sorry for the carelessness. It was added. For details, please refer to line 313.

14. Secondary inorganic aerosol is typically referred to as SIA in the literature. Consider using the same nomenclature.

Reply: Accepted with thanks. Revisions were made throughout the manuscript.

14. Section 3.4.1: What is the correlation coefficient for the observed/modelled ozone?

Reply: Thanks for the question. The slope and R^2 of linear regression between the observed and modelled ozone was 0.87 and 0.60, respectively. Since index of agreement (IOA) is often used to evaluate the model performance, we used IOA in the manuscript.

15. Figure 11: For reporting PMF profiles, it would be easier if the authors split the profiles by episode-non-episode. The current plots are difficult to interpret since there is a lot of information on the same plot.

Reply: Thanks for the suggestion. Since the data collected in episodes and non-episodes were combined to conduct source apportionment analysis in the revised manuscript, the average profiles in summer and autumn were given separately (Figures 10 and 11), which looked better.

For details, please refer to Figures 10 and 11.

References:

Zhang, F., Wang, Z.W., Cheng, H.R., Lv, X.P., Gong, W., Wang, X.M., and Zhang, G., 2015. Seasonal variations and chemical characteristics of PM_{2.5} in Wuhan, central China. *Sci. Total Environ.* 518, 97-105.

1 Chemical characteristics and causes of airborne particulate pollution in warm
2 seasons in Wuhan, central China

3

4 X.P. Lyu ¹, N. Chen ², H. Guo ^{1*}, L.W. Zeng ¹, W.H. Zhang ³, F. Shen ², J.H. Quan ², N. Wang ⁴

5 ¹ Department of Civil and Environmental Engineering, The Hong Kong Polytechnic University,
6 Hong Kong

7 ² Hubei Provincial Environment Monitoring Center, Wuhan, China

8 ³ Department of Environmental Sciences, School of Resource and Environmental Sciences,
9 Wuhan University, Wuhan, China

10 ⁴ Guangdong Provincial Key Laboratory of Regional Numerical Weather Prediction, Institute of
11 Tropical and Marine Meteorology, Guangzhou, China

12 *Corresponding author. Tel: +852 3400 3962; Fax: +852 2334 6389; Email:
13 ceguohai@polyu.edu.hk

14

15 **Abstract:** Continuous measurements of airborne particles and their chemical compositions were
16 conducted in May, June, October, and November 2014 at an urban site in Wuhan, central China.
17 The results indicate that particle concentrations remained at a relatively high level in Wuhan,
18 with averages of 135.1 ± 4.4 (mean \pm 95% confidence interval) and $118.9 \pm 3.7 \mu\text{g}/\text{m}^3$ for PM_{10}
19 and 81.2 ± 2.6 and $85.3 \pm 2.6 \mu\text{g}/\text{m}^3$ for $\text{PM}_{2.5}$ in summer and autumn, respectively. Moreover,
20 $\text{PM}_{2.5}$ levels frequently exceeded the National Standard Level II (i.e., daily average of $75 \mu\text{g}/\text{m}^3$),
21 and six $\text{PM}_{2.5}$ episodes (i.e., daily $\text{PM}_{2.5}$ averages above $75 \mu\text{g}/\text{m}^3$ for 3 or more consecutive days)
22 were captured during the sampling campaign. Potassium was the most abundant element in $\text{PM}_{2.5}$,
23 with an average concentration of $2060.7 \pm 82.3 \text{ ng}/\text{m}^3$; this finding indicates intensive biomass
24 burning in and around Wuhan during the study period, because almost no correlation was found
25 between potassium and mineral elements (iron and calcium). The source apportionment results
26 confirm that biomass burning was the main cause of episodes 1, 3, and 4, with contributions to
27 $\text{PM}_{2.5}$ of $46.6\% \pm 3.0\%$, $50.8\% \pm 1.2\%$, and $44.8\% \pm 2.6\%$, respectively, whereas fugitive dust
28 was the leading factor in episode 2. Episodes 5 and 6 resulted mainly from increases in vehicular
29 emissions and secondary inorganic aerosols, and the mass and proportion of NO_3^- both peaked
30 during episode 6. The high levels of NO_x and NH_3 and the low temperature during episode 6
31 were responsible for the increase of NO_3^- . Moreover, the formation of secondary organic carbon

32 was found to be dominated by aromatics and isoprene in autumn, and the contribution of
33 aromatics to secondary organic carbon increased during the episodes.

34 **Keywords:** PM_{2.5}; NO₃⁻; SOA; biomass burning; formation mechanism

35

36 **1. Introduction**

37 Airborne particulate pollution, also called “haze,” has swept across China in recent years,
38 particularly over its northern, central, and eastern parts (Cheng et al., 2014; Kang et al., 2013;
39 Wang et al., 2013). Due to its detrimental effects on human health (Anderson et al., 2012;
40 Goldberg et al., 2001), the atmosphere (Yang et al., 2012; White and Roberts, 1977), acid
41 precipitation (Zhang et al., 2007; Kerminen et al., 2001), and climate change (Ramanathan et al.,
42 2001; Nemesure et al., 1995), particulate pollution has become a major concern of scientific
43 communities and local governments. China’s national ambient air quality standards issued in
44 2012 regulate the annual upper limit of PM₁₀ (i.e., particulate matter with an aerodynamic
45 diameter of less than 10 μm) and PM_{2.5} (i.e., particulate matter with an aerodynamic diameter of
46 less than 2.5 μm) as 70 μg/m³ and 35 μg/m³ and 24-h averages as 150 μg/m³ and 75 μg/m³,
47 respectively (GB 3095-2012).

48 Numerous studies have been conducted in China to understand the spatiotemporal variations in
49 particle concentrations, the chemical compositions, and the causes of haze events (Cheng et al.,
50 2014; Cao et al., 2012; Zheng et al., 2005; Yao et al., 2002). In general, particulate pollution is
51 more severe in winter due to additional emissions (e.g., coal burning) and unfavorable dispersion
52 conditions (Lyu et al., 2015a; Zheng et al., 2005). Northern China often suffers heavier, longer,
53 and more frequent haze pollution than southern China (Cao et al., 2012). Chemical analysis
54 indicates that secondary inorganic aerosol (SIA; i.e., sulfate [SO₄²⁻], nitrate [NO₃⁻], and
55 ammonium [NH₄⁺]) and secondary organic aerosol (SOA) dominate the total mass of airborne
56 particles (Zhang et al., 2014; Zhang et al., 2012). However, the composition differs among the
57 size-segregated particles. In general, secondary species and mineral or sea salt components are
58 prone to be apportioned in fine and coarse particles (Zhang et al., 2013; Theodosi et al., 2011).
59 Indeed, the general characteristics of particles (e.g., toxicity, radiative forcing, acidity) are all
60 tightly associated with their chemical compositions and physical sizes, which therefore have
61 been extensively studied in the field of aerosols. To better understand and control airborne
62 particulate pollution, the causes and formation mechanisms have often been investigated (Wang

63 et al., 2014a and b; Kang et al., 2013; Oanh and Leelasakultum, 2011). Apart from the
64 unfavorable meteorological conditions, emission enhancement was often the major culprit. There
65 is little doubt that industrial and vehicular emissions contributed greatly to the particle mass via
66 direct emission and secondary formation of particles from gaseous precursors, such as sulfur
67 dioxide (SO₂), nitrogen oxides (NO_x), and volatile organic compounds (VOCs; Guo et al., 2011a).
68 In addition, some other sources in specific regions or during specific time periods have also built
69 up the particle concentrations to a remarkable degree, e.g., coal combustion in north China (Cao
70 et al., 2005; Zheng et al., 2005) and biomass burning in Southeast Asia (Deng et al., 2008; Koe et
71 al., 2001). Furthermore, some studies have explored the possible formation mechanisms of the
72 main particle components (SIA and SOA) and distinguished the contributions of different
73 formation pathways. For example, Wang et al. (2014) demonstrated that heterogeneous oxidation
74 of SO₂ on aerosol surfaces was an important supplementary pathway to particle-bound SO₄²⁻ in
75 addition to gas phase oxidation and reactions in clouds. In contrast, it was reported that
76 homogeneous and heterogeneous reactions dominated the formation of NO₃⁻ during the day and
77 night, respectively (Pathak et al., 2011; Lin et al., 2007; Seinfeld and Pandis, 1998). Furthermore,
78 biogenic VOCs and aromatics were shown to be the main precursors of SOA (Kanakidou et al.,
79 2005; Forstner et al., 1997).

80 Despite numerous studies, the full components of airborne particles have seldom been reported
81 due to the cost of sampling and chemical analysis, resulting in a gap in our understanding of the
82 chemical characteristics of particles. In addition, although the causes of particle episodes have
83 been discussed in many case studies (Wang et al., 2014; Deng et al., 2008), the contributions
84 have rarely been quantified. Furthermore, the formation mechanisms might differ in various
85 circumstances. Therefore, an overall understanding of the chemical characteristics of airborne
86 particles, the causes of the particle episodes, and the formation mechanisms of the enhanced
87 species would be of great value. In addition, the frequent occurrence of haze pollution has
88 become a regular phenomenon in central China during warm seasons, but the causes have not
89 been identified and the contributions have not been quantified. Wuhan is the largest megacity in
90 central China and has suffered from severe particulate pollution in recent years. The data indicate
91 that the frequency of days in which PM_{2.5} exceeded the national standard level II (i.e., a daily
92 average of 75 µg/m³) in Wuhan reached 55.1% in 2014 (Wuhan Environmental Bulletin, 2014).
93 In the warm seasons of 2014, the hourly maximum PM_{2.5} (564 µg/m³) was even higher than that

94 in winter ($383 \mu\text{g}/\text{m}^3$), as shown in [Figure S1](#) in the Supplementary Material. Moreover, because
95 the air quality in Wuhan is strongly influenced by the surrounding cities, the pollution level in
96 Wuhan also reflects the status of the city clusters in central China. However, previous studies
97 ([Lyu et al., 2015a](#); [Cheng et al., 2014](#)) did not allow a complete understanding of the properties
98 of airborne particles in this region, particularly during the warm seasons, nor could they guide
99 control strategies. It is therefore urgent to understand the chemical characteristics of airborne
100 particles and to explore the causes and formation mechanisms of the particle episodes in Wuhan.
101 This study deeply analyzed the chemical characteristics of $\text{PM}_{2.5}$ in Wuhan from a full suite of
102 component measurement data: SO_4^{2-} , NO_3^- , NH_4^+ , organic carbon (OC), including primary
103 organic carbon (POC) and secondary organic carbon (SOC), elemental carbon (EC), and metal
104 elements. Furthermore, based on the analysis of meteorological conditions, chemical signatures,
105 source apportionment, and distribution of wildfires, the causes of the $\text{PM}_{2.5}$ episodes are
106 identified and their contributions quantified. Finally, this study used a photochemical box model
107 incorporating a master chemical mechanism (PBM-MCM) and theoretical calculation to
108 investigate the formation processes of NO_3^- and SOC. Ours is the first study to quantify the
109 contribution of biomass burning to $\text{PM}_{2.5}$ and examine the formation mechanisms of both
110 inorganic and organic components in $\text{PM}_{2.5}$ in central China.

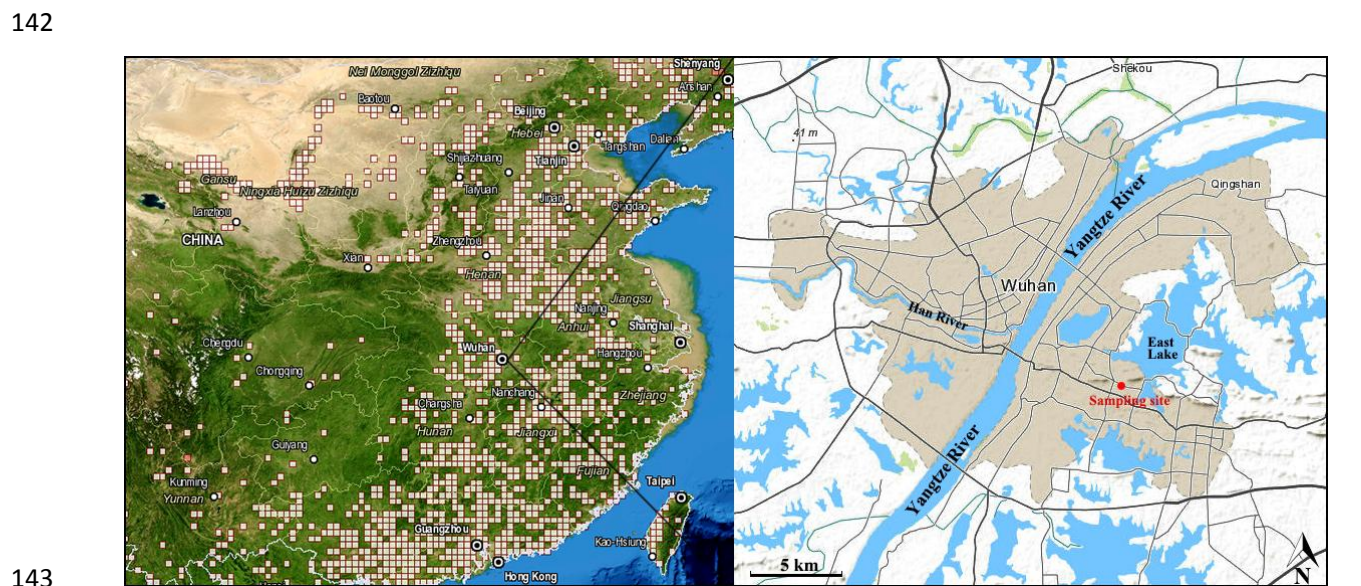
111

112 **2. Methods**

113 **2.1 Data collection**

114 The whole set of air pollutants were continuously monitored at an urban site in the largest
115 megacity of central China, i.e., Wuhan. The measurement covered two periods: May and June in
116 summer and October and November in autumn of 2014. The measured species included particle-
117 phase pollutants such as PM_{10} , $\text{PM}_{2.5}$, and particle-bound components and gas-phase pollutants,
118 including VOCs, SO_2 , CO, NO, NO_2 , O_3 , HNO_3 (g), NH_3 (g), and HCl (g). **Hourly data were**
119 **obtained for each species.** The sampling site (30.54°N , 114.37°E) was located in the Hubei
120 Environmental Monitoring Center Station, as shown in [Figure 1](#), located in a mixed commercial
121 and residential area in which industries are seldom permitted. The instruments were housed in a
122 room in a six-story building (~ 18 m above ground level) adjacent to a main road at a straight-line
123 distance of ~ 15 m. **The traffic volume of the road was around 200 vehicles per hour. However, a**
124 **wall (~ 2 m high) and several rows of trees (7 to 8 m high) were located between the road and the**

125 **sampling site.**
126 PM₁₀ and PM_{2.5} were measured with a continuous ambient particulate monitor (Thermo Fisher-
127 1405D, USA) **integrated with a filter dynamics measurement system to minimize the loss of**
128 **semivolatile particulate matter.** The water-soluble ions (WSIs) in PM_{2.5} and gases including
129 HNO₃, HCl, and NH₃ were detected with an online ion chromatography monitor (Metrohm-
130 MARGA 1S, Switzerland) and an aerosol OC/EC online analyzer (Sunset-RT-4, USA); **the**
131 **NIOSH thermal-optical transmission method** was used to resolve the carbonaceous aerosols (OC
132 and EC). In addition, the elements in PM_{2.5} were measured with a customized metal analyzer.
133 **This instrument used a PM_{2.5} impactor to collect the airborne particulate samples, which were**
134 **analyzed by the β-ray in terms of mass concentrations. The filters loaded with particles were then**
135 **sent to an x-ray fluorescence analysis system for quantitative analysis.** For the analysis of trace
136 gases (SO₂, CO, NO, NO₂, and O₃), we used a suite of commercial analyzers developed by
137 Thermo Environmental Instruments Inc., which have been described in detail (Lyu et al. 2016;
138 Geng et al., 2009). Furthermore, a gas chromatography–flame ionization detector–mass
139 spectrometry system (TH_PKU-300) was used to resolve the real time data of the ambient VOCs.
140 The details of the analysis techniques, resolution, detection limits, and the protocol of quality
141 assurance/control were provided by Lyu et al. (2016) and Wang et al. (2014).

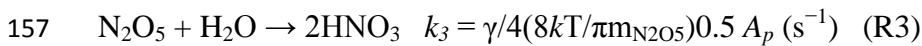
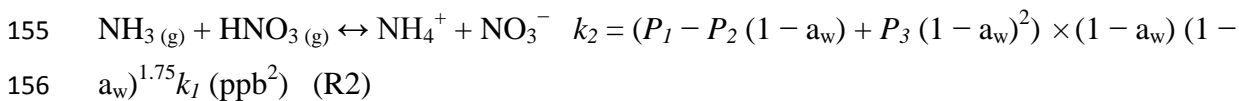
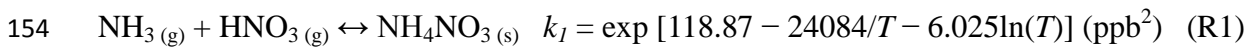


144 Figure 1. Geographic location of the sampling site. White blocks in left panel represent total
145 distribution of **wildfires** in autumn 2014, and urban area in Wuhan is highlighted in gray in the
146 right panel.

147

148 **2.2 Theoretical calculation and model simulation**

149 Theoretical calculation and model simulation were applied in this study to examine the formation
150 mechanisms of NO_3^- and SOC. The particle-bound NO_3^- was generally combined with NH_3 or
151 presented as HNO_3 in the ammonia-deficient environment, following the processes described in
152 R1 through R3 after HNO_3 was formed by the oxidation of NO_x (Pathak et al., 2011, Lin et al.,
153 2010). The production of NO_3^- can be calculated with Equations 1-4.



$$158 \ln(P_I) = -135.94 + 8763/T + 19.12 \ln(T) \quad (\text{Eq.1})$$

$$159 \ln(P_2) = -122.65 + 9969/T + 16.22 \ln(T) \quad (\text{Eq.2})$$

$$160 \ln(P_3) = -182.61 + 13875/T + 24.46 \ln(T) \quad (\text{Eq.3})$$

$$161 [\text{NO}_3^-] = 0.775 \left(\frac{[\text{NH}_3] + [\text{HNO}_3] - \sqrt{([\text{NH}_3] + [\text{HNO}_3])^2 - 4([\text{NH}_3][\text{HNO}_3] - k_1(k_2))}}{2} \right) \quad (\text{Eq.4})$$

162 where R1 and R2 describe the homogeneous formation of NO_3^- in humidity conditions lower
163 and higher than the deliquescence relative humidity of NH_4NO_3 (i.e., 62%; Tang and Munkelwitz,
164 1993), respectively. R3 presents the heterogeneous reaction of N_2O_5 on the preexisting aerosol
165 surfaces. k_{I-3} represents the rate of reactions R1-3. T , a_w , and P are the temperature, the relative
166 humidity, and the temperature-related coefficient, respectively. In R3, γ is the reaction
167 probability of N_2O_5 on aerosol surfaces, assigned as 0.05 and 0.035 on the surface of sulfate
168 ammonia and element carbon, respectively (Aumont et al., 1999; Hu and Abbatt, 1997). k is the
169 Boltzmann constant (1.38×10^{-23}), $m_{\text{N}_2\text{O}_5}$ is the molecular mass of N_2O_5 (1.79×10^{-22} g), and A_p
170 is the aerosol specific surface area (cm^2/cm^3).

171 Furthermore, the PBM-MCM model was used to simulate the oxidation products in this study,
172 i.e., O_3 , N_2O_5 , the semi-volatile oxidation products of VOCs (SVOCs), and radicals such as OH,
173 HO_2 , and RO_2 . With full consideration of photochemical mechanisms and real meteorological
174 conditions, the model has been successfully applied in the study of photochemistry. Details about
175 the model construction and application were published by Lyu et al. (2015b), Ling et al. (2014),
176 and Lam et al. (2013).

177 **2.3 Source apportionment model**

178 The positive matrix factorization (PMF) model (EPA PMF v5.0) was used to resolve the sources
179 of PM_{2.5}. As a receptor model, PMF has been extensively used in the source apportionment of
180 airborne particles and VOCs (Brown et al., 2007; Lee et al., 1999). Detailed introductions of the
181 model can be found in Paatero (1997) and Paatero and Tapper (1994). Briefly, it decomposes the
182 input matrix (X) into matrices of factor contribution (G) and factor profile (F) in *p* sources, as
183 shown in Equation 5. The hourly concentrations of PM_{2.5} components were included in the input
184 matrix. Values below the detection limit (DL; see Table S1 in the Supplement) were replaced
185 with DL/2. The uncertainties were $\sqrt{(10\% \times \text{concentration})^2 + \text{DL}^2}$ and 5/6×DL for the
186 samples with concentrations higher and lower than DL, respectively. Samples with any missing
187 values were excluded. In total, 807 and 806 samples were applied for source apportionment in
188 summer and autumn, respectively.

189 The selection of the factor number and the best solution depended upon the following criteria. (1)
190 A lower Q value (Equation 6; a function to evaluate the model runs) was preferable. (2) The ratio
191 between Q_{robust} and Q_{true} was lower than 1.5. In this study, the ratios were 0.8 and 0.9 for the
192 summer and autumn data simulation, respectively. (3) Good agreement was shown between the
193 predicted and observed PM_{2.5}. The slope and correlation coefficient (R²) for the linear regression
194 were 0.91 and 0.86 in summer and 0.95 and 0.98 in autumn, respectively, as shown in Figure S2
195 in the Supplement. The lower R² value seen during the summer might be due to the lack of WSI
196 data. (4) The residuals were normally distributed between -3 and 3. Table S2 summarizes the
197 percentage of samples with residuals between -3 and 3 for each species; the lowest percentages
198 were 92.9% and 96.0% for Ni in summer and autumn, respectively. The scaled residuals for
199 PM_{2.5} are shown in Figure S3 in the Supplement. The percentage of residuals between -3 and 3
200 was comparable between summer (97.5%) and autumn (98.1%). Finally (5), no correlation was
201 found between the factors, which was achieved by examining the G-space plots and controlled
202 by the FPEAK model runs. Figures S4 and S5 in the Supplement present the G-space plots in
203 summer and autumn, respectively. The low factor contributions and poor correlations indicated
204 that rotational ambiguity was effectively controlled.

205 A bootstrap method was used to estimate the model errors, according to which 95% confidence
206 intervals (CIs) were calculated. The 95% CI for PM_{2.5} was 0.6 μg/m³ (0.7% of predicted PM_{2.5})
207 in summer and 2.6 μg/m³ (3.2% of predicted PM_{2.5}) in autumn.

208
$$x_{ij} = \sum_{k=1}^p g_{ik} f_{kj} + e_{ij} \quad (\text{Eq.5})$$

209
$$Q = \sum_{i=1}^n \sum_{j=1}^m \left[\frac{x_{ij} - \sum_{k=1}^p g_{ik} f_{kj}}{u_{ij}} \right]^2 \quad (\text{Eq.6})$$

210 where x_{ij} and u_{ij} are the concentration and uncertainty of j species (total of m) in i sample (total
 211 of n), g_{ik} represents the contribution of k_{th} source to i sample, f_{kj} indicates the fraction of j
 212 species in k_{th} source, and e_{ij} is the residual for j species in the i sample.

213

214 **3. Results and discussion**

215 **3.1 Concentrations of PM₁₀ and PM_{2.5}**

216 **Table 1** shows the mean concentrations of PM₁₀ and PM_{2.5} in Wuhan and other Chinese cities and
 217 regions. The mean, maximum and minimum values, and standard deviation or 95% CI were
 218 provided if available. In general, the concentrations of airborne particles in Wuhan (135.1 ± 4.4
 219 and $118.9 \pm 3.7 \mu\text{g}/\text{m}^3$ for PM₁₀; 81.2 ± 2.6 and $85.3 \pm 2.6 \mu\text{g}/\text{m}^3$ for PM_{2.5} in summer and
 220 autumn, respectively) were lower than those in northern China (i.e., Beijing and Xi'an),
 221 comparable to those in eastern China (i.e., Shanghai and Nanjing), and higher than those in
 222 southern China (i.e., Guangzhou and Hong Kong) and Taiwan. **Bearing in mind that** the sampling
 223 site, period, method, and instrument all interfere with comparisons, the ambient particulate
 224 pollution in Wuhan was severe.

225 From summer to autumn, PM₁₀ levels declined considerably from 135.1 ± 4.4 to 118.9 ± 3.7
 226 $\mu\text{g}/\text{m}^3$, whereas PM_{2.5} remained statistically stable ($p > 0.05$). **The higher summer PM₁₀**
 227 **concentration was probably related to a higher load of fugitive dust. In Wuhan, the temperature**
 228 **($25.6 \text{ }^\circ\text{C} \pm 0.2 \text{ }^\circ\text{C}$) in summer was considerably higher than that ($17.5 \text{ }^\circ\text{C} \pm 0.3 \text{ }^\circ\text{C}$) in autumn ($p <$**
 229 **0.05), which led to lower water content in the soil and a higher tendency of dust suspension. In**
 230 **addition, the average wind speed in summer (1.2 ± 0.04 vs. 0.8 ± 0.03 m/s in autumn) was also**
 231 **higher ($p < 0.05$), which could also have favored the generation of fugitive dust.**

232

233 Table 1. Comparisons of PM₁₀ and PM_{2.5} (in $\mu\text{g}/\text{m}^3$) between Wuhan and other Chinese cities and
 234 regions.

	PM ₁₀	PM _{2.5}	Sampling period
Wuhan	$135.1 \pm 4.4^{\text{I}}$	$81.2 \pm 2.6^{\text{I}}$	May-Jun. 2014 (this study)
	$118.9 \pm 3.7^{\text{I}}$	$85.3 \pm 2.6^{\text{I}}$	Oct.-Nov. 2014 (this study)
Beijing	155.9^{II}	73.8^{II}	Jun.-Aug. 2009 ^a

	194.4 ^{II}	103.9 ^{II}	Sept.-Nov. 2009 ^a
	133.7 ± 87.8 ^{III}	71.5 ± 53.6 ^{III}	2012 whole year ^b
Xi'an	257.8 ± 194.7 ^{III}	140.9 ± 108.9 ^{III}	2011 whole year ^c
Shanghai	97.4 to 149.2 ^{IV}	62.3 to 103.1 ^{IV}	Jul. 2009-Sept. 2010 ^d
Nanjing	119 to 171 ^{IV}	87 to 125 ^{IV}	Jun. 2012 ^e
Guangzhou	23.4 ^{II}	19.2 ^{II}	Jun.-Aug. 2010-2013 ^f
	51.0 ^{II}	41.3 ^{II}	Sept.-Nov. 2010-2013 ^f
Hong Kong	31.0 ± 16.7 ^{III}	17.7 ± 12.9 ^{III}	Jun.-Aug. 2014 ^g
	55.8 ± 23.6 ^{III}	34.0 ± 17.3 ^{III}	Sept.-Nov. 2014 ^g
Taiwan	39.5 ± 11.6 ^{III}	21.8 ± 7.5 ^{III}	May-Nov. 2011 ^h

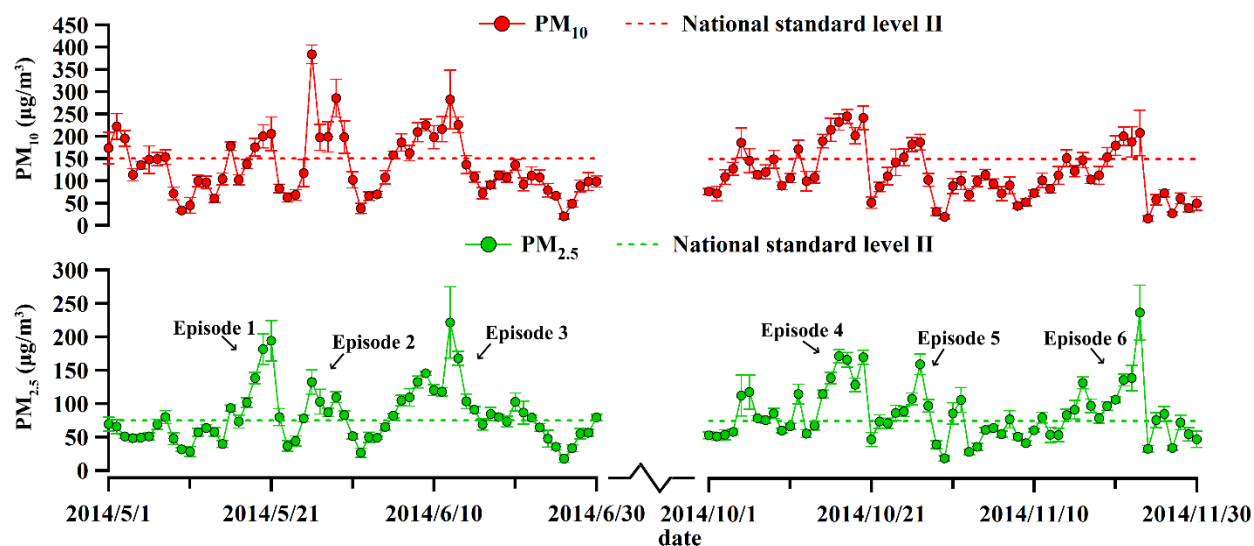
235 ^I mean ± 95% confidence interval; ^{II} arithmetic mean; ^{III} mean ± standard deviation; ^{IV} range.

236 ^a Liu et al. (2014); ^b Liu et al. (2015); ^c Wang et al. (2015); ^d Wang et al. (2013); ^e Shen et al.
 237 (2014); ^f Deng et al. (2015); ^g HKEPD (2014); ^h Gugamsetty et al. (2012).

238
 239 Figure 2 presents the daily concentrations of PM₁₀ and PM_{2.5} during the sampling period in
 240 Wuhan, with the National Standard Level II (daily averages of 150 and 75 µg/m³ for PM₁₀ and
 241 PM_{2.5}, respectively). It was found that the concentrations of PM₁₀ and PM_{2.5} frequently exceeded
 242 the standard levels, indicating the significance of ambient particulate pollution in Wuhan.
 243 Because smaller particles tend to pose more harm to human health and to the atmosphere due to
 244 their larger specific surface areas (Yang et al., 2012; Goldberg et al., 2001), and because the
 245 chemical compositions in PM₁₀ were not analyzed, this study focused mainly on PM_{2.5}. During
 246 the sampling campaign, six PM_{2.5} episodes, named episodes 1 through 6, with daily averages of
 247 PM_{2.5} in excess of 75 µg/m³, were captured (Figure 2). It should be noted that to ensure the data
 248 size of each episode, only the cases in which the daily PM_{2.5} average was consecutively higher
 249 than 75 µg/m³ for 3 days or longer were treated as PM_{2.5} episodes.

250 Table 2 summarizes the concentrations of PM₁₀ and PM_{2.5} and the percentage of PM_{2.5} in PM₁₀,
 251 referred to as PM_{2.5}/PM₁₀, during the summer and autumn episodes and non-episodes. PM₁₀ and
 252 PM_{2.5} concentrations increased significantly ($p < 0.05$) during the episodes in both summer and
 253 autumn. The PM_{2.5}/PM₁₀ value also increased remarkably on episode days compared to that on
 254 non-episode days, except for episode 2 (45.9% ± 2.5%), which suggests that more secondary
 255 species and/or primary fine particles (e.g., primary OC and EC generated from combustion) were

256 generated or released during the episodes. In contrast, the lower $PM_{2.5}/PM_{10}$ value during
 257 episode 2 might imply a strong source of coarse particles. Indeed, this inference was confirmed
 258 by the source apportionment analysis in section 3.3.3.
 259



260
 261 Figure 2. Daily concentrations of PM_{10} and $PM_{2.5}$ in May, June, October, and November 2014.
 262 Episode 1, May 16 to 22; episode 2, May 25 to 30; episode 3, June 5 to 15; episode 4, October
 263 15 to 20; episode 5, October 24 to 28; Episode 6, November 14 to 23.

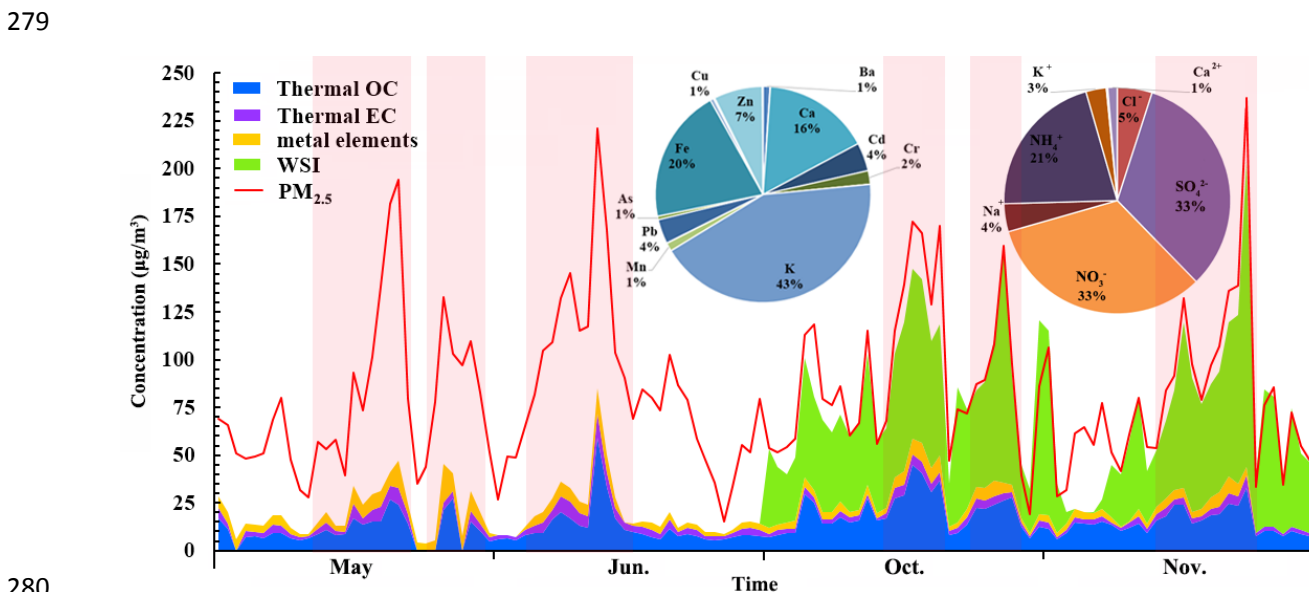
264
 265 Table 2. Mean PM_{10} , $PM_{2.5}$, and $PM_{2.5}/PM_{10}$ with 95% CI during $PM_{2.5}$ episodes and non-
 266 episodes in Wuhan. Non-episode 1 and Non-episode 2 represent the non-episode periods in
 267 summer and autumn, respectively.

	PM_{10} ($\mu\text{g}/\text{m}^3$)	$PM_{2.5}$ ($\mu\text{g}/\text{m}^3$)	$PM_{2.5}/PM_{10}$ (%)
Episode 1	154.3 \pm 10.1	123.0 \pm 9.1	72.8 \pm 2.6
Episode 2	230.1 \pm 19.1	98.9 \pm 5.7	45.9 \pm 2.5
Episode 3	191.4 \pm 9.8	126.7 \pm 7.0	66.9 \pm 1.8
Non-episode 1	98.5 \pm 3.9	56.6 \pm 1.7	58.9 \pm 1.5
Episode 4	221.8 \pm 8.9	148.6 \pm 5.2	67.9 \pm 2.0
Episode 5	154.2 \pm 10.4	108.2 \pm 6.8	69.3 \pm 3.1
Episode 6	157.3 \pm 9.0	120.0 \pm 7.6	71.2 \pm 2.1
Non-episode 2	88.7 \pm 3.4	64.2 \pm 2.2	65.3 \pm 1.3

268

269 3.2 Chemical composition of PM_{2.5}

270 Figure 3 shows the daily variations of PM_{2.5} and its composition. As the instrument for the
271 analysis of WSIs was initially deployed in September 2014, data are not available for May and
272 June. The carbonaceous aerosol ($18.5 \pm 1.2 \mu\text{g}/\text{m}^3$) and elements ($6.0 \pm 0.3 \mu\text{g}/\text{m}^3$) accounted for
273 $19.1\% \pm 0.6\%$ and $6.2\% \pm 0.2\%$ of PM_{2.5} in summer, respectively. In autumn, WSIs were the
274 most abundant component in PM_{2.5} ($64.4 \pm 2.5 \mu\text{g}/\text{m}^3$; $68.6\% \pm 1.9\%$), followed by carbonaceous
275 aerosol ($24.3 \pm 1.0 \mu\text{g}/\text{m}^3$; $25.5\% \pm 0.8\%$) and elements ($4.5 \pm 0.2 \mu\text{g}/\text{m}^3$; $4.6\% \pm 0.1\%$). The
276 secondary inorganic ions SO_4^{2-} ($18.8 \pm 0.6 \mu\text{g}/\text{m}^3$), NO_3^- ($18.7 \pm 0.8 \mu\text{g}/\text{m}^3$), and NH_4^+ ($12.0 \pm$
277 $0.4 \mu\text{g}/\text{m}^3$) dominated the WSIs, with the average contribution of $34.0\% \pm 0.6\%$, $30.1\% \pm 0.5\%$,
278 and $20.4\% \pm 0.1\%$, respectively.

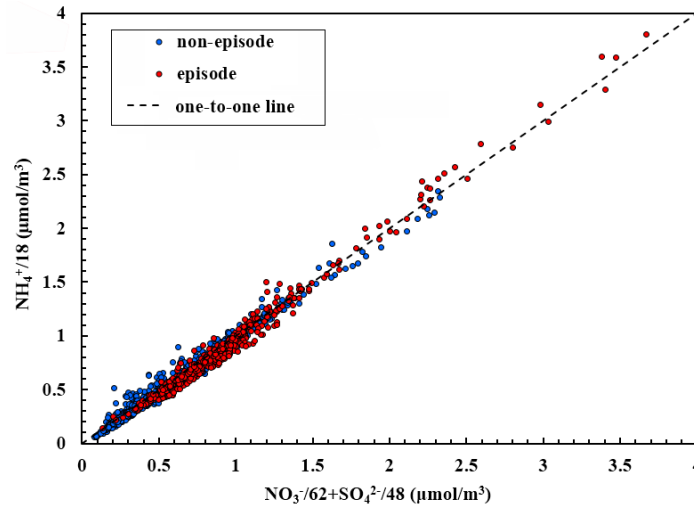


280
281 Figure 3. Daily variations of PM_{2.5} and its components. Pie charts represent the composition of
282 elements and water-soluble ions, respectively. Pink shaded areas represent episodes.

283
284 The charge balance between the anions and cations was usually used to predict the existing forms
285 of SIAs and the acidity of PM_{2.5}. Figure 4 shows the relative abundance of molar charges of SIAs,
286 which were located fairly close to the one-to-one line on both episode and non-episode days.
287 This finding suggests that NH_4NO_3 and $(\text{NH}_4)_2\text{SO}_4$ were coexisting forms of the SIAs in PM_{2.5} in
288 Wuhan. When extending NH_4^+ to total cations (NH_4^+ , Ca^{2+} , Mg^{2+} , Na^+ , and K^+) and NO_3^- and
289 SO_4^{2-} to total anions (NO_3^- , SO_4^{2-} , and Cl^-), the molar charges of the cations and anions were
290 balanced (slope, 0.98; $R^2 = 0.98$), as shown in Figure S6 in the Supplement, indicating that PM_{2.5}

291 was neutralized during autumn in Wuhan.

292



293

294 Figure 4. Relative abundance of molar charges of PM_{2.5} during autumn in Wuhan.

295

296 For the carbonaceous aerosol, OC ($14.8 \pm 0.5 \mu\text{g}/\text{m}^3$) and EC ($3.6 \pm 0.1 \mu\text{g}/\text{m}^3$) accounted for
297 $79.9\% \pm 0.3\%$ and $20.2\% \pm 0.3\%$ of the total carbon, respectively. In general, SOC was expected
298 to exist when the OC/EC ratio was greater than 2 (Duan et al., 2005; Chow et al., 1996), and the
299 proportion of SOC increased with the increase in OC/EC ratio. The average OC/EC ratio was 4.8
300 ± 0.1 in Wuhan, which suggests that SOC (i.e., carbon fraction of SOA) was an important
301 component in PM_{2.5}. Indeed, as the constituents of OC, SOC and POC can be distinguished with
302 the EC-tracer method, following Equations 7 and 8 (Cabada et al., 2004):

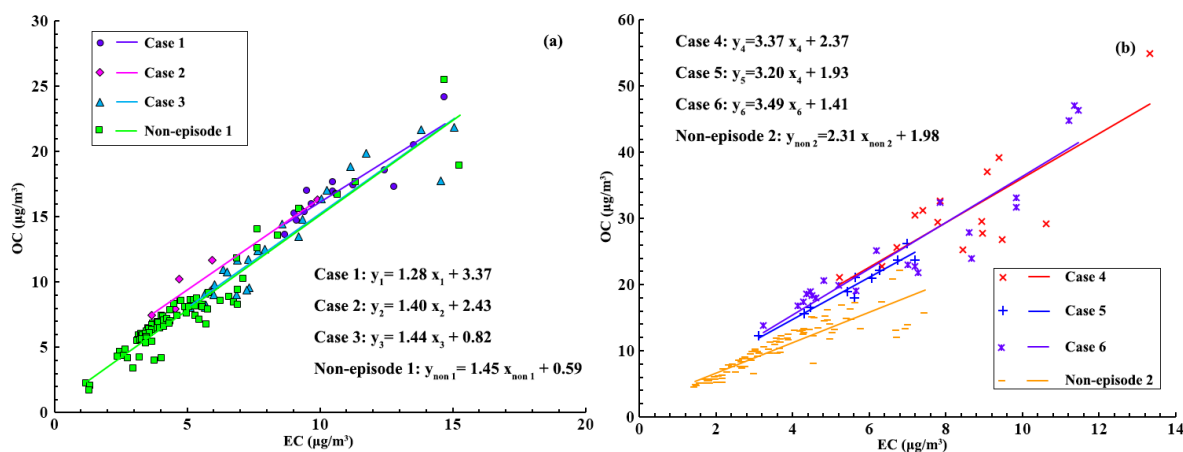
303
$$\text{POC} = (\text{OC}/\text{EC})_{\text{prim}} \times \text{EC} + \text{OC}_{\text{non-comb}} \quad (\text{Eq.7})$$

304
$$\text{SOC} = \text{OC} - \text{POC} \quad (\text{Eq.8})$$

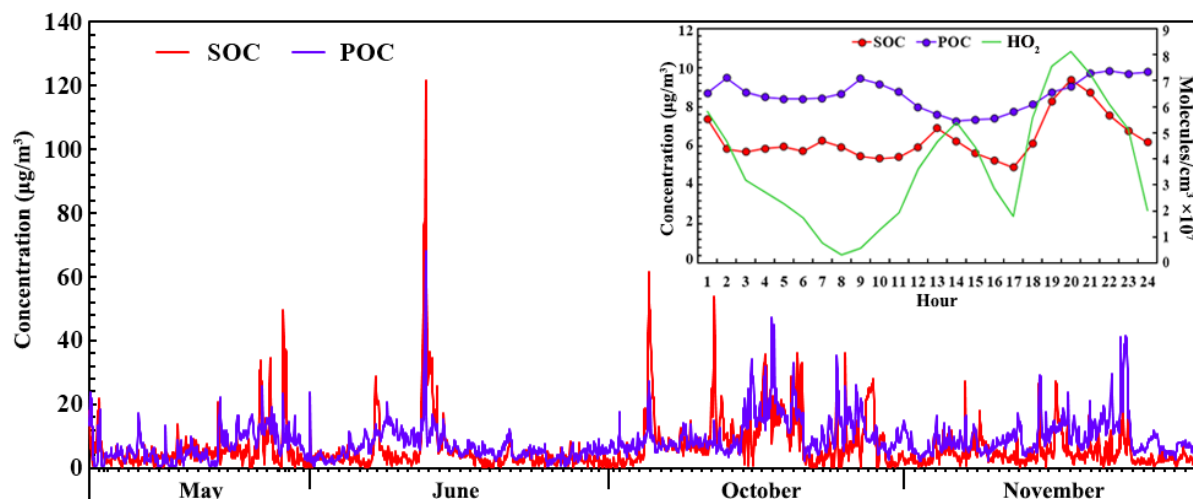
305 where $(\text{OC}/\text{EC})_{\text{prim}}$ was the ratio of primary OC to EC, obtained from the pairs of OC and EC
306 with the OC/EC ratios among the 10% lowest; and $\text{OC}_{\text{non-comb}}$ was the primary OC that was not
307 related to combustion activities. These values were determined by the slope and intercept of the
308 linear regression between primary OC and EC, respectively (Figure 5). Because the abundance
309 of SOC depended largely upon the oxidative capacity of the atmosphere, the oxidative radical
310 (HO_2) was simulated with the PBM-MCM model and compared with the pattern of SOC. More
311 details about the simulation are provided in section 3.4. Figure 6 shows the hourly concentrations
312 of SOC and POC and the average diurnal patterns of SOC, POC, and HO_2 . In general, the POC
313 levels ($8.6 \pm 0.2 \mu\text{g}/\text{m}^3$) were slightly higher than those of SOC ($6.4 \pm 0.3 \mu\text{g}/\text{m}^3$; $p < 0.05$). The

314 difference was greatest in November, when the concentration was 9.5 ± 0.4 and $4.7 \pm 0.3 \mu\text{g}/\text{m}^3$
 315 for POC and SOC, respectively. Because the production of SOC was closely related to the
 316 atmospheric oxidative capacity, the lowest fraction of SOC in November might be attributable to
 317 the weakest oxidative capacity; for example, the O_3 level was lowest in November (14.3 ± 1.0
 318 ppbv). **Two peaks were found for the simulated diurnal pattern of HO_2 , which might be caused**
 319 **by strong solar radiation at noon and in the early afternoon and by reactions among alkenes and**
 320 **O_3 and NO_3 at night (Emmerson et al., 2005; Kanaya et al., 1999).** The diurnal patterns of POC
 321 and SOC revealed that POC levels were relatively stable throughout the day. The increase in the
 322 POC level in the early morning (06:00 to 08:00) and late afternoon and early evening (16:00 to
 323 20:00) was likely related to increases in vehicular emissions during rush hours, and the decrease
 324 from 08:00 to 15:00 might be caused by the extension of the boundary layer. In contrast, the
 325 SOC level showed two peaks at around 12:00 and 19:00, which was consistent with the diurnal
 326 variation of the simulated HO_2 , suggesting that the formation of SOC was closely related to the
 327 oxidative radicals in the atmosphere. (A detailed relationship is discussed in section 3.4.3.)

328



329 Figure 5. Regression between OC and EC with the 10% lowest OC/EC ratios during (a) summer
 330 and (b) autumn in Wuhan.
 331



332
 333 Figure 6. Hourly concentrations of SOC and POC. Insert graph presents average diurnal
 334 variations of SOC, POC, and HO₂.

335
 336 Among the elements, potassium (K; $2060.7 \pm 82.3 \text{ ng/m}^3$), iron (Fe; $996.5 \pm 34.3 \text{ ng/m}^3$), and
 337 calcium (Ca; $774.1 \pm 39.4 \text{ ng/m}^3$) were the most abundant species, accounting for $47.0\% \pm 2.2\%$,
 338 $21.4\% \pm 0.3\%$, and $15.6\% \pm 0.3\%$ of the total analyzed elements, respectively. Correlation
 339 analysis indicated that Fe had good correlation with Ca ($R^2 = 0.66$; Figure S7 in the Supplement),
 340 whereas weak correlations of K with Fe ($R^2 = 0.14$) and Ca ($R^2 = 0.09$) were found, suggesting
 341 that Fe and Ca shared common sources that were different from the sources of K. Because Fe
 342 and Ca are typical crustal elements, fugitive dust (e.g., dust from traffic, construction and
 343 demolition works, yards, and bare soil) was their most likely source. In contrast, apart from
 344 emissions from mineral sources, K is also emitted from biomass burning. As such, K was
 345 believed to be mainly emitted from biomass burning in this study, which is further supported by
 346 the moderate correlations of K with OC ($R^2 = 0.52$) and EC ($R^2 = 0.48$) because biomass burning
 347 also emits OC and EC (Saarikoski et al., 2007; Echalar et al., 1995).

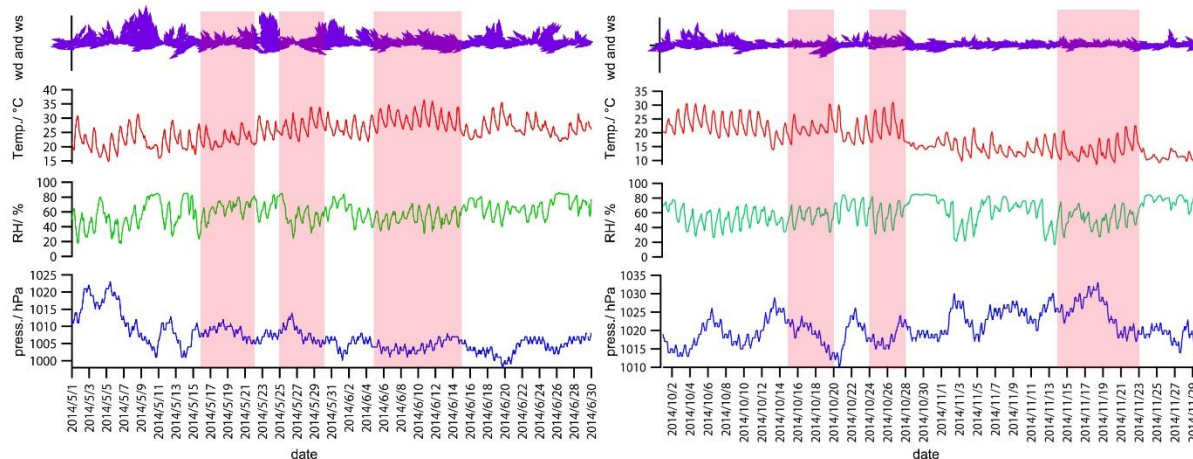
348 3.3 Causes of PM_{2.5} episodes

349 3.3.1 Meteorological conditions

350 The processes of particle formation, dispersion, and deposition are closely related to
 351 meteorological conditions. To interpret the possible causes of the PM_{2.5} episodes, Figure 8 shows
 352 the patterns of wind direction and speed, temperature, relative humidity, and atmospheric
 353 pressure in Wuhan during the monitoring period. In general, southeast winds prevailed at the
 354 sampling site with a wind speed of approximately 1.0 m/s. The low wind speed indicates the

355 dominance of local air masses. However, due to the high stability and long lifetime of PM_{2.5}, the
 356 regional and superregional impact could not be eliminated. In comparison with those in summer,
 357 the wind speed (summer, 1.1 ± 0.04 m/s; autumn, 0.8 ± 0.03 m/s) and temperature (summer, 25.6
 358 ± 0.2 m/s; autumn, 17.5 ± 0.3 m/s) were significantly ($p < 0.05$) lower in autumn, whereas the
 359 atmospheric pressure (summer, 1006.9 ± 0.2 hPa; autumn, 1020.9 ± 0.2 hPa) was much higher.
 360 During the episodes, the wind speed was generally lower than during non-episodes, with the
 361 exception of episode 5. This might be one cause for the episodes, but it does not fully explain the
 362 great enhancements of PM_{2.5}, because the wind speeds were very low and the differences
 363 between the episodes and non-episodes were minor. The atmospheric pressure was not very high
 364 during episodes 1 through 5, suggesting that the synoptic system was not responsible for the
 365 occurrence of these PM_{2.5} episodes. **However, the atmospheric pressure was remarkably higher**
 366 **($p < 0.05$) in episode 6 (1024 ± 1 hPa) than in non-episode 2 (1021 ± 0.3 hPa), which might have**
 367 **suppressed the diffusion of PM_{2.5} and the gaseous precursors. In addition, the temperature was**
 368 **lower (episode 6, 14.0 °C ± 0.4 °C; non-episode 2, 17.2 °C ± 0.3 °C; $p < 0.05$), which favors the**
 369 **gas-to-particle partitioning of semivolatile and non-thermal stabilized species. As a consequence,**
 370 **these effects might have elevated the PM_{2.5} concentrations in episode 6, which is discussed**
 371 **further in section 3.4.2.**

372



373

374 Figure 8. Meteorological patterns in Wuhan during the monitoring period. Pink shaded areas
 375 represent PM_{2.5} episodes.

376

377 3.3.2 Chemical signatures

378 Table 3 summarizes the mass concentrations and percentages of the main components in PM_{2.5}.
379 The mass concentrations of PM_{2.5} components significantly increased from non-episode days to
380 episode days ($p < 0.05$). In contrast, the percentages of the chemical components in PM_{2.5} varied
381 by species. In summer, the fractions of EC and K in PM_{2.5} experienced significant increases from
382 non-episode 1 (EC, 4.8% \pm 0.2%; K, 2.0% \pm 0.1%) to episode 1 (EC, 5.7% \pm 0.5%; K, 4.4% \pm
383 0.3%) and episode 3 (EC, 5.3% \pm 0.2%; K, 3.0% \pm 0.2%). Because EC is the tracer of
384 incomplete combustion (Chow et al., 1996) and K is the indicator of biomass burning (Saarikoski
385 et al., 2007; Echalar et al., 1995), the higher percentages of EC and K in episodes 1 and 3 imply
386 the outstanding contribution of biomass burning. In contrast, the fraction of OC in PM_{2.5}
387 remained stable on both episode and non-episode days ($p > 0.05$), possibly because the high
388 temperatures in summer hindered the gas-to-particle partitioning of semivolatile organics
389 (Takekawa et al., 2003). Furthermore, the percentages of Ca (2.9% \pm 0.4%) and Fe (2.7% \pm 0.3%)
390 significantly increased during episode 2 ($p < 0.05$) compared to those in non-episode 1 (Ca, 1.1%
391 \pm 0.1%; Fe, 1.5% \pm 0.1%), which shows that fugitive dust made a considerable contribution to
392 PM_{2.5} in episode 2. In addition, biomass burning might also have contributed to PM_{2.5}, in view of
393 the increase in the percentage of K (non-episode 1, 2.0% \pm 0.1%; episode 2, 3.2% \pm 0.2%).
394 In autumn, the percentage of K significantly ($p < 0.05$) increased during episode 4 (3.1% \pm 0.1%
395 vs. 2.1% \pm 0.1% in non-episode 2), as did that of OC (27.3% \pm 0.7% vs. 20.9% \pm 0.8% in non-
396 episode 2), suggesting the dominant role of biomass burning in episode 4. Furthermore, the
397 fractions of OC in episode 5 (23.8% \pm 1.5%) and NO₃⁻ in episode 6 (26.1% \pm 1.0%) were
398 obviously higher than those in non-episode 2 (OC, 20.9% \pm 0.8%; NO₃⁻, 19.8% \pm 0.9%). Due to
399 the complexity of the sources of OC and NO₃⁻, the causes of episodes 5 and 6 are further
400 explored in the following sections.
401 In summary, episodes 1, 3, and 4 were greatly affected by biomass burning. This finding was
402 further confirmed by the significant increases in the gaseous tracers of biomass burning such as
403 ethyne (C₂H₂) and methyl chloride (CH₃Cl) (Guo et al., 2011b; Simoneit et al., 2002) during
404 these episodes ($p < 0.05$; see Figure S8 in the Supplement).

Table 3. Concentrations ($\mu\text{g}/\text{m}^3$) and percentages (in parentheses) of the main components of $\text{PM}_{2.5}$ during non-episodes and episodes. Bold font demonstrates significant increase in percentage of $\text{PM}_{2.5}$ components during episodes compared to non-episodes.

	Summer				Autumn			
	Episode 1	Episode 2	Episode 3	Non-episode 1	Episode 4	Episode 5	Episode 6	Non-episode 2
OC	18.5±1.3 (15.1%±0.8%)	16.3±3.3 (14.0%±1.9%)	19.8±2.5 (14.5%±1.0%)	7.9±0.3 (15.4%±0.7%)	35.1±1.7 (27.3%±0.7%)	24.9±1.9 (23.8%±1.5%)	22.7±1.5 (21.4%±0.8%)	14.6±1.0 (20.9%±0.8%)
EC	6.8±0.5 (5.7%±0.5%)	4.3±0.6 (4.1%±0.5%)	6.6±0.5 (5.3%±0.2%)	2.8±0.1 (4.8%±0.2%)	5.4±0.4 (4.2%±0.3%)	4.2±0.4 (4.1%±0.4%)	4.2±0.4 (3.9%±0.2%)	2.7±0.2 (4.0%±0.2%)
SO_4^{2-}	NA	NA	NA	NA	28.3±0.9 (22.8%±0.9%)	25.9±2.4 (23.7%±1.1%)	21.3±2.0 (19.2%±0.6%)	18.8±0.9 (26.9%±0.9%)
NO_3^-	NA	NA	NA	NA	23.7±1.9 (17.8%±0.9%)	24.7±2.9 (21.4%±1.1%)	30.8±3.6 (26.1%±1.0%)	15.8±1.3 (19.8%±0.9%)
NH_4^+	NA	NA	NA	NA	16.5±0.8 (12.9%±0.2%)	15.6±1.8 (13.7%±0.6%)	16.8±1.8 (14.5%±0.3%)	11.0±0.7 (14.9%±0.3%)
K	5.3±0.6 (4.4%±0.3%)	3.4±0.4 (3.2%±0.2%)	3.8±0.5 (3.0%±0.2%)	1.1±0.1 (2.0%±0.1%)	4.0±0.2 (3.1%±0.1%)	2.3±0.2 (2.2%±0.1%)	2.4±0.2 (2.2%±0.1%)	1.4±0.1 (2.1%±0.1%)
Ca	1.2±0.4 (1.1%±0.1%)	3.2±0.4 (2.9%±0.4%)	0.9±0.3 (0.8%±0.1%)	0.6±0.04 (1.1%±0.1%)	1.1±0.1 (0.9%±0.1%)	0.8±0.2 (0.8%±0.2%)	0.8±0.1 (0.8%±0.1%)	0.3±0.04 (0.5%±0.1%)
Fe	1.4±0.1 (1.3%±0.1%)	2.8±0.3 (2.7%±0.3%)	1.1±0.1 (1.0%±0.1%)	0.8±0.05 (1.5%±0.1%)	1.5±0.1 (1.2%±0.2%)	1.2±0.2 (1.2%±0.2%)	1.2±0.1 (1.1%±0.1%)	0.6±0.04 (0.9%±0.1%)

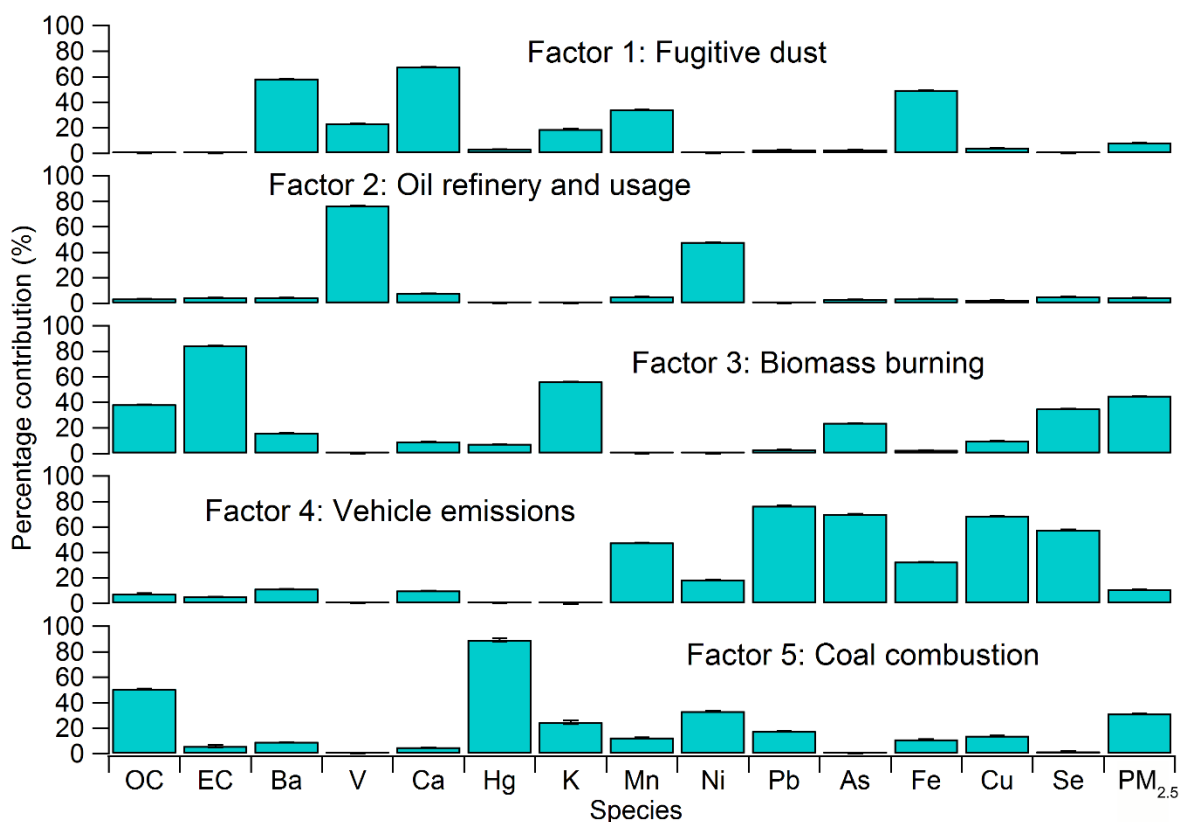
384 3.3.3 Source apportionment

385 To clarify the sources of PM_{2.5} and quantify their contributions, the hourly data on PM_{2.5}
386 components were applied to PMF for source apportionment. Five and six sources were resolved
387 for summer and autumn, respectively, as shown in Figure 10 and Figure 11. The source of SIA
388 was missing in summer, due to the lack of WSI data. For other sources, the profile of each
389 corresponding source was similar in summer and autumn. Factor 1 had high loadings of crustal
390 elements (i.e., Ba, Ca, Mn, and Fe), indicating the source of fugitive dust. Factor 2 was likely
391 associated with oil refinery and usage, in view of the high percentages of V and Ni, which often
392 originate from the combustion of heavy oil (Barwise et al., 1990; Nriagu and Pacyna, 1988).
393 Factor 3 was distinguished by the high loadings of OC, EC, and K, indicating the biomass
394 burning source (Zhang et al., 2013; Friedli et al., 2003). Factor 4 seemed to represent vehicle
395 emissions, due to the dominance of Pb, As, Cu, and Se. Cu is the tracer of road traffic because it
396 is widely used as the antioxidant in brake pads (de Fatima Andrade et al., 2012). Although lead-
397 containing gasoline has been forbidden in China since 2000, high levels of Pb are often reported
398 in traffic sources (Yang et al., 2013; Song et al., 2012), which might be due to the use of Pb-
399 containing materials in car components, such as lead wheel weights, solder in electronics, and
400 lead-acid batteries (Song et al., 2012). OC and Hg dominated in factor 5, and Cl⁻ also showed
401 high loading in this factor in the autumn profile. It is well documented that Hg and Cl⁻ are
402 largely emitted from coal combustion (Wang et al., 2010; Ye et al., 2003). Hence, this factor was
403 assigned as coal combustion. Finally, a source of SIA with high loadings of NO₃⁻, SO₄²⁻, and
404 NH₄⁺ was resolved in autumn.

405 Figures S9 and S10 in the Supplement show the day-to-day variations of the source contributions
406 in summer and autumn, respectively. Overall, biomass burning was the largest contributor (45.0%
407 ± 0.03%) to PM_{2.5} in summer. However, the contribution of biomass burning in autumn (23.7% ±
408 0.5%) was lower than that of SIA (38.6% ± 0.7%). Bearing in mind the uncertainties caused by
409 the lack of WSIs, the greater contribution of biomass burning in summer might be associated
410 with the lower WSIs. For example, NO₃⁻ was expected to be much lower in summer due to its
411 thermal decomposition at high temperatures. Table 4 summarizes the source contributions during
412 episodes and non-episodes. Noticeably, the contributions of biomass burning were significantly
413 higher (*p* < 0.05) in episode 1 (59.2 ± 6.3 μg/m³; 46.6% ± 3.0%), episode 3 (64.9 ± 3.3 μg/m³;
414 50.8% ± 1.2%), and episode 4 (48.7 ± 2.9 μg/m³; 44.8% ± 2.6%) than those in the corresponding

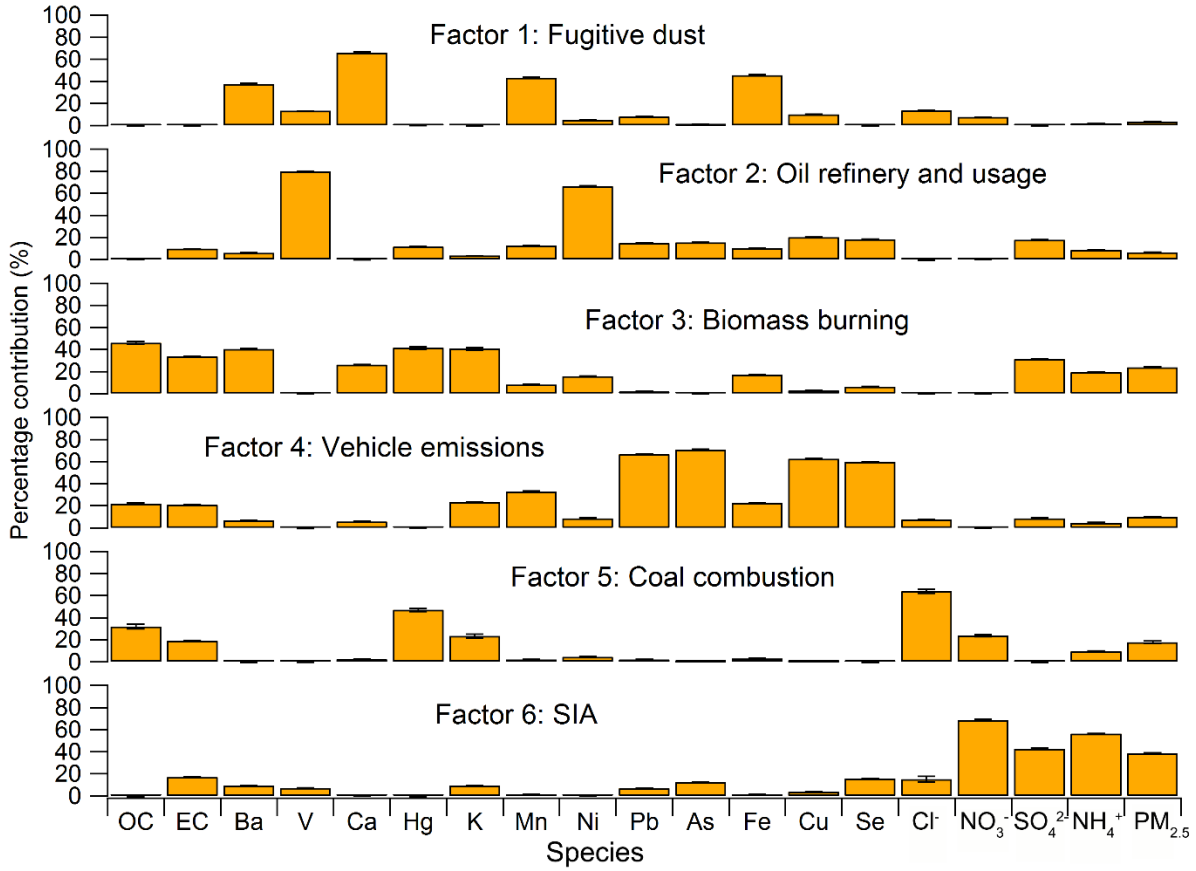
415 non-episodes, confirming that biomass burning was the main cause of these PM_{2.5} episodes. In
 416 addition, vehicle emissions made a greater contribution to episode 4 ($14.9 \pm 1.2 \mu\text{g}/\text{m}^3$; $13.7\% \pm$
 417 1.1%) than to non-episode 2. In contrast, the contribution of fugitive dust ($6.5 \pm 1.3 \mu\text{g}/\text{m}^3$; 5.6%
 418 $\pm 1.0\%$) in episode 2 was remarkably ($p < 0.05$) higher than in non-episode 1 ($1.1 \pm 0.1 \mu\text{g}/\text{m}^3$;
 419 $1.8\% \pm 0.2\%$). This finding was consistent with the inference that episode 2 was attributable to
 420 fugitive dust according to the low PM_{2.5}/PM₁₀ ratio ($45.9\% \pm 2.5\%$) and high levels of crustal
 421 elements (Ca, $2.9\% \pm 0.4\%$; Fe, $2.7\% \pm 0.3\%$) in this episode. In addition, vehicle emissions and
 422 SIA both experienced significant increases in episodes 5 and 6 ($p < 0.05$). In fact, the increase of
 423 OC in episode 5 (see Table 3) was mainly caused by vehicle emissions and coal combustion
 424 (Table S3 in the Supplement). For episode 6, in addition to the increase in OC, SIA was also an
 425 important contributor, particularly for NO₃⁻, which increased from $9.9 \pm 1.2 \mu\text{g}/\text{m}^3$ in non-
 426 episode 2 to $21.4 \pm 3.3 \mu\text{g}/\text{m}^3$ in episode 6 (Table S3).

427



428

429 Figure 10. Profiles of PM_{2.5} sources in summer. Error bars represent 95% CI estimated by
 430 bootstrap method in PMF.



431

432 Figure 11. Profiles of PM_{2.5} sources in autumn. Error bars represent 95% CI estimated by

433 bootstrap method in PMF.

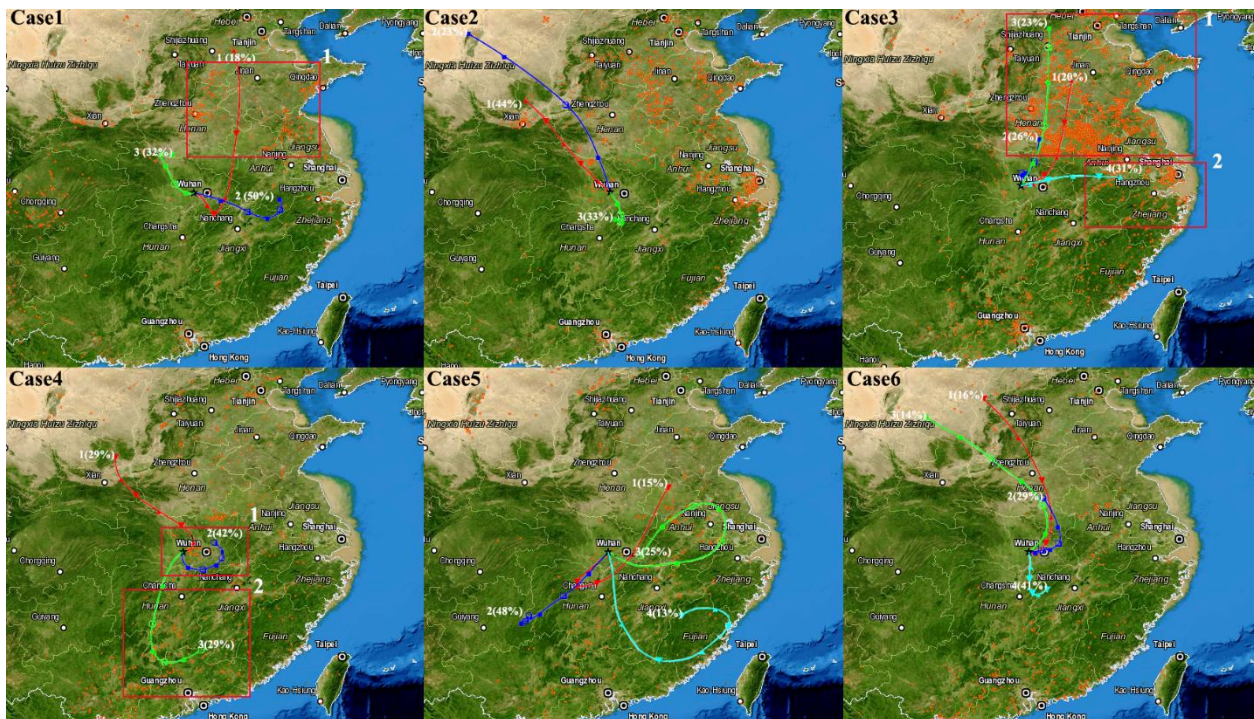
Table 4. Mass concentration ($\mu\text{g}/\text{m}^3$) and percentage contribution (in parentheses) of sources to sum of resolved species in $\text{PM}_{2.5}$. Bold font represents a significant increase in percentage contribution in episodes compared to non-episodes.

	Fugitive dust	Oil refinery and usage	Biomass burning	Vehicle emissions	Coal Combustion	SIA
Episode 1	10.0 \pm 1.3 (8.7% \pm 1.2%)	4.0 \pm 1.2 (2.8% \pm 0.7%)	59.2\pm6.3 (46.6% \pm3.0%)	12.2 \pm 1.8 (9.6% \pm 1.2%)	36.0 \pm 2.7 (32.2% \pm 2.5%)	—
Episode 2	29.5\pm6.1 (27.5% \pm5.5%)	8.2 \pm 2.6 (6.7% \pm 1.7%)	37.1 \pm 5.8 (35.3% \pm 4.8%)	10.8 \pm 3.1 (11.9% \pm 3.2%)	20.9 \pm 4.7 (18.7% \pm 3.1%)	—
Episode 3	6.4 \pm 0.5 (5.3% \pm 0.4%)	4.9 \pm 1.0 (3.9% \pm 0.7%)	64.9\pm3.3 (50.8% \pm1.2%)	8.8 \pm 0.9 (7.9% \pm 0.9%)	41.6 \pm 3.3 (32.1% \pm 1.5%)	—
Non-episode 1	4.8 \pm 0.6 (8.7% \pm 1.0%)	2.9 \pm 0.4 (5.0% \pm 0.7%)	22.2 \pm 1.6 (35.2% \pm 1.9%)	9.3 \pm 0.6 (16.3% \pm 1.0%)	19.5 \pm 1.0 (35.9% \pm 1.7%)	—
Episode 4	3.3 \pm 0.3 (3.0% \pm 0.2%)	7.2 \pm 0.6 (7.0% \pm 0.8%)	48.7\pm2.9 (44.8% \pm2.6%)	14.9\pm1.2 (13.7% \pm1.1%)	13.8 \pm 1.7 (11.9% \pm 1.3%)	23.3 \pm 3.3 (19.6% \pm 2.6%)
Episode 5	2.3 \pm 0.5 (2.7% \pm 0.5%)	5.3 \pm 0.6 (6.6% \pm 0.8%)	21.1 \pm 2.8 (22.1% \pm 2.3%)	12.2\pm1.9 (13.85\pm2.1%)	14.8 \pm 2.0 (17.5% \pm 2.7%)	39.9\pm6.4 (37.2% \pm3.0%)
Episode 6	2.6 \pm 0.3 (3.0% \pm 0.3%)	4.7 \pm 0.6 (4.7% \pm 0.4%)	18.4 \pm 2.4 (21.2% \pm 2.5%)	14.2\pm1.3 (16.1% \pm1.3%)	17.7 \pm 2.5 (16.3% \pm 1.7%)	44.6\pm6.8 (38.7% \pm2.2%)
Non-episode 2	0.9 \pm 0.1 (1.6% \pm 0.2%)	4.7 \pm 0.3 (8.6% \pm 0.6%)	22.2 \pm 1.6 (39.3% \pm 2.5%)	4.2 \pm 0.4 (7.4% \pm 0.7%)	9.8 \pm 0.8 (18.1% \pm 1.8%)	20.5 \pm 2.5 (25.0% \pm 2.3%)

430 **3.3.4 Open fires and air mass trajectories**

431 To further confirm the biomass burning activities during the PM_{2.5} episodes, the **wildfire**
432 distribution (downloaded from NASA Firms Web Fire Mapper, and accessible at
433 <https://firms.modaps.eosdis.nasa.gov/firemap/>) and 72-h backward air mass trajectories
434 (simulated by Hysplit v4.9 model) are plotted in **Figure 12**. **Because the concentrations,**
435 **compositions and source contributions of PM_{2.5} were averaged over the entire period of each**
436 **episode, the wildfire distribution and backward trajectories were also averaged for the entire**
437 **period of each episode.** Consistent with the great contributions to PM_{2.5} of biomass burning, the
438 air masses arriving in Wuhan had passed over the areas where **intensive** open fires were detected
439 in episodes 1, 3, and 4. In episode 2, wildfires were **widespread** in northeast China. However, the
440 air mass trajectories were mainly from the south and northwest and evaded the burning areas,
441 which might explain why biomass burning was not a predominant factor in episode 2. The sparse
442 wildfires in episodes 5 and 6 coincided with the source apportionment result that biomass
443 burning did not significantly elevate the concentration of PM_{2.5}.

444



445

446 **Figure 12. Wildfire** distribution and 72-h backward air mass trajectories. Red squares
447 demonstrate potential areas where biomass burning aggravated particulate pollution in Wuhan.

448

449 3.4 Formation mechanisms

450 3.4.1 Model validation

451 In this study, the PBM-MCM model was used to help investigate the formation mechanisms of
452 NO_3^- and SOC. Before application, the model was validated via O_3 simulation. **Figure S11**
453 compares the daily averages and diurnal variations of O_3 between the simulation and the
454 observations. It was found that the model simulated O_3 variation well in both daily and diurnal
455 patterns. However, it generally overestimated the O_3 levels in November. The meteorological
456 parameters indicated that the frequency of foggy days was extremely high (36.7%) in November,
457 possibly resulting in a weakening of solar radiation and consequently of photochemical reactivity.
458 To quantitatively evaluate the performance of the model, the index of agreement (IOA) was
459 calculated using Equation 9.

$$460 \quad \text{IOA} = 1 - \frac{\sum_{i=1}^n (O_i - S_i)^2}{\sum_{i=1}^n (|O_i - \bar{O}| + |S_i - \bar{O}|)^2} \quad (\text{Eq.9})$$

461 where \bar{O} is the average of n samples and O_i and S_i represent the observed and simulated values,
462 respectively. Within the interval of [0, 1], higher IOA values indicated better agreement between
463 the simulation and observation.

464 By calculation, the IOA reached 0.86, indicating excellent performance of the model in the O_3
465 simulation. Because O_3 production is closely associated with oxidative radicals, intermediates,
466 and products, the robust O_3 simulation gave us full confidence to accept the simulated N_2O_5 ,
467 HO_2 , and SVOCs.

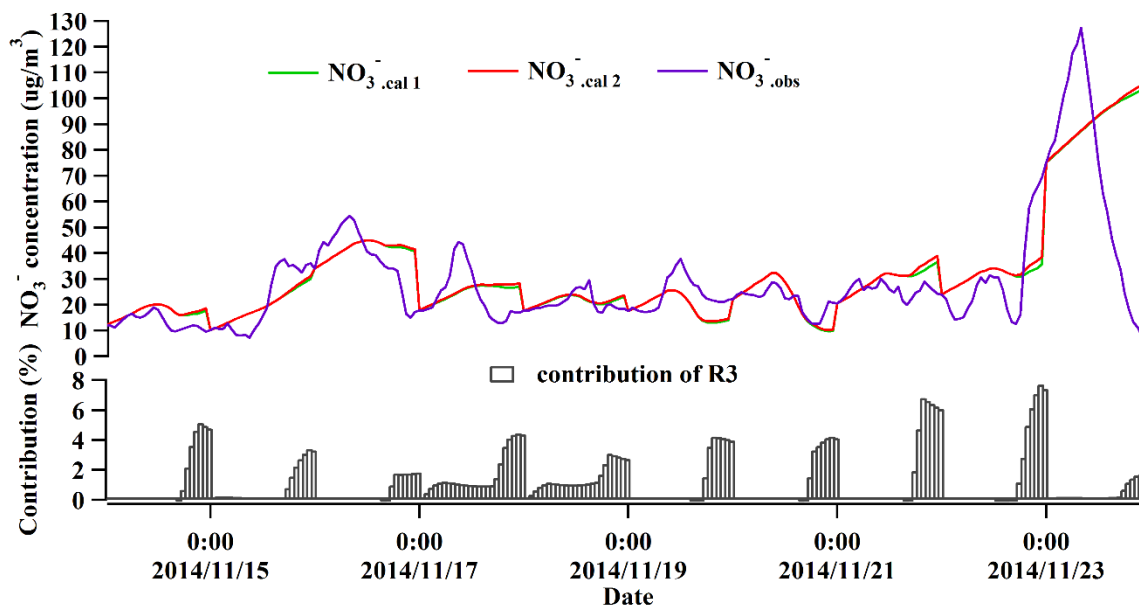
468

469 3.4.2 NO_3^- formation

470 The composition analysis indicated that the proportion of NO_3^- increased remarkably during
471 episode 6. To interpret this phenomenon, the formation mechanisms of NO_3^- were investigated.
472 **Figure 14** shows the hourly variations of the calculated and observed NO_3^- and the contribution
473 of R3 (i.e., $\text{N}_2\text{O}_5 + \text{H}_2\text{O} \rightarrow 2\text{HNO}_3$), among which $\text{NO}_3^-_{\text{cal 1}}$, $\text{NO}_3^-_{\text{cal 2}}$, and $\text{NO}_3^-_{\text{obs}}$ referred to
474 homogeneous formation (R1 and R2), total formation (R1, R2, and R3), and field measurement
475 of NO_3^- , respectively. Although the particle-bound NO_3^- was influenced by many factors (i.e.,
476 formation, deposition, and dispersion), the calculations generally well reproduced the measured
477 NO_3^- in episode 6, with a high correlation coefficient ($R^2 = 0.63$) and an IOA of 0.78. However,
478 on November 23, 2014, the observed NO_3^- decreased rapidly from 09:00, which was not
479 captured by the calculations. This discrepancy was likely caused by the weather conditions on

480 that day, because (1) the average wind speed increased from 1.7 m/s before 09:00 to 2.7 m/s after
481 09:00 and even reached 4.0 m/s at 14:00; and (2) moderate rain began at 12:00 and continued
482 until 23:00, with total precipitation of 24 mm. Indeed, this was the beginning of a 7-day rainy
483 period, which ended episode 6 with a sharp decrease of the PM_{2.5} concentration (approximately
484 175 µg/m³; see [Figure 2](#)).

485 Because the values of NO₃⁻_{cal 1} were very close to those of NO₃⁻_{cal 2}, the variation of NO₃⁻ in
486 episode 6 could be well explained by the homogeneous formation (R1 and R2), whereas the
487 heterogeneous reaction of N₂O₅ on aerosol surfaces (R3) made only a minor contribution to the
488 total NO₃⁻ (i.e., nearly nil from 0:00 to 17:00 and 3.7% ± 0.6% from 18:00 to 23:00). Because
489 the homogeneous formation of NO₃⁻ was closely related to the concentrations of HNO₃ (g) and
490 NH₃ (g) and the temperature (see R1 and R2), [Table 4](#) compares the temperature, HNO₃ (g), NH₃
491 (g), NO, NO₂, O₃, and the simulated OH and HO₂ (a measure of oxidative capacity [[Cheng et al.,](#)
492 [2010](#)]) between episode 6 and non-episode 2. It was found that the levels of HNO₃ (g) (0.65 ±
493 0.01 ppbv) and NH₃ (g) (13.48 ± 0.72 ppbv) in episode 6 were significantly higher than those
494 during the non-episode 2 (0.47 ± 0.03 and 9.54 ± 0.37 ppbv for HNO₃ and NH₃, respectively),
495 which might substantially favor the formation of NH₄NO₃. Because HNO₃ (g) is generally
496 formed by oxidation of NO_x, the production of HNO₃ (g) should be closely related to the
497 oxidative capacity of the air and the level of NO_x. In episode 6, the levels of O₃ (17.09 ± 2.04
498 ppbv), OH ([3.8 ± 1.3] × 10⁵ molecules/cm³), and HO₂ ([1.1 ± 0.3] × 10⁷ molecules/cm³) were
499 noticeably lower than those in non-episode 2 (O₃, 24.57 ± 1.64 ppbv; OH, [7.2 ± 0.9] × 10⁵
500 molecules/cm³; HO₂, [2.0 ± 0.2] × 10⁷ molecules/cm³), indicating a weaker oxidative capacity.
501 However, the levels of NO (43.55 ± 11.65 ppbv) and NO₂ (44.93 ± 2.29 ppbv) were much higher
502 than those in non-episode 2 (14.70 ± 2.40 and 29.46 ± 0.95 ppbv for NO and NO₂, respectively),
503 possibly leading to the enhancement of HNO₃ (g) in episode 6. Furthermore, the particle-bound
504 NO₃⁻ was of low thermal stability ([Querol et al., 2004](#)), and the temperature lowered ~2.3 C ° in
505 episode 6, which suppressed the decomposition and volatilization of NH₄NO₃. Therefore, the
506 high levels of NO_x and NH₃ and the low temperature were both responsible for the increase in
507 NO₃⁻ in episode 6.



508

509 Figure 14. Comparison of NO_3^- between theoretical calculations and observation in episode 6.

510

511 Table 4. Comparison of temperature, HNO_3 (g), NH_3 (g), NO, NO_2 , O_3 , and simulated OH and
 512 HO_2 between episode 6 and non-episode 2.

	Episode 6	Non-episode 2
Temperature ($^{\circ}\text{C}$)	14.9 ± 0.5	17.2 ± 0.3
HNO_3 (ppbv)	0.65 ± 0.01	0.47 ± 0.03
NH_3 (ppbv)	13.48 ± 0.72	9.54 ± 0.37
NO (ppbv)	43.55 ± 11.65	14.70 ± 2.40
NO_2 (ppbv)	44.93 ± 2.29	29.46 ± 0.95
O_3 (ppbv)	17.09 ± 2.04	24.57 ± 1.64
OH (molecules/ cm^3)	$(3.8 \pm 1.3) \times 10^5$	$(7.2 \pm 0.9) \times 10^5$
HO_2 (molecules/ cm^3)	$(1.1 \pm 0.3) \times 10^7$	$(2.0 \pm 0.2) \times 10^7$

513

514 3.4.3 SOC formation

515 In addition to the high levels of NO_3^- in episode 6, the proportions of OC also increased during
 516 the autumn episodes. Because SOC is an important fraction in OC that often grows as an air
 517 mass ages, it could help to explain the increase of OC in the autumn episodes by exploring the
 518 possible formation mechanisms of SOC. It is well known that SOC formation is closely related

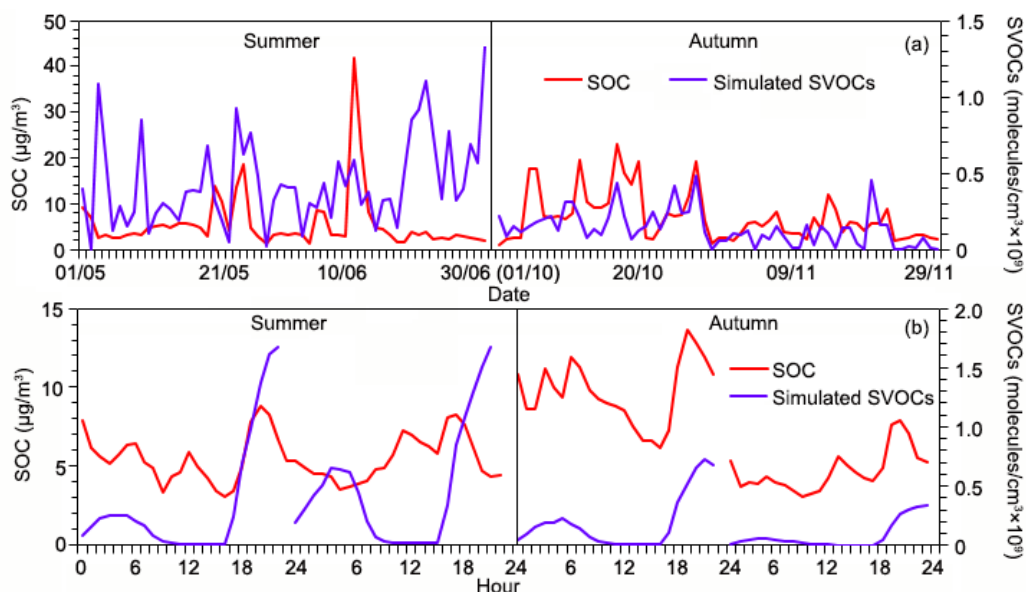
519 to SVOCs, which are formed from the reactions with oxidative radicals (i.e., RO_2 , NO_3 , and HO_2 ;
520 Kanakidou et al., 2005; Forstner et al., 1997). Hence, the relationship between SOC and SVOCs
521 was investigated. The SVOCs were simulated with the PBM-MCM model and SOC was
522 calculated with the EC-tracer method mentioned in section 3.2.1. The speciation of SVOCs and
523 their precursors can be found in the Table S4 in the Supplementary Material. Briefly, the
524 precursors of SVOCs include isoprene, aromatics, and C_7 - C_{12} n-alkanes.

525 Figure 15 presents the daily and diurnal variations in SOC and SVOCs. It was found that SOCs
526 correlated well with SVOCs in both daily ($R^2 = 0.52$) and diurnal ($R^2 = 0.63$) patterns in autumn,
527 indicating that the simulated SVOCs were responsible for the production of SOC. The oxidation
528 products of aromatics and isoprene were the main constituents of the SVOCs, with average
529 contributions of $42.5\% \pm 2.8\%$ and $39.4\% \pm 2.0\%$, respectively. Among the aromatics, xylenes
530 made the greatest contribution ($15.0\% \pm 0.7\%$) to the SVOCs, followed by trimethylbenzenes
531 ($11.5\% \pm 0.7\%$), ethylbenzene ($8.8\% \pm 0.5\%$), toluene ($5.1\% \pm 0.7\%$), and benzene ($2.2\% \pm$
532 0.2%). Compared to those in non-episode 2 (i.e., $40.7\% \pm 3.4\%$ and $41.1\% \pm 2.4\%$ contributed
533 by aromatics and isoprene, respectively), the contribution of aromatics to SVOCs increased to
534 $46.3\% \pm 4.1\%$ during the episodes, whereas the proportion of isoprene oxidation products
535 decreased to $36.1\% \pm 3.7\%$, suggesting that the increase in aromatics was the main cause of the
536 autumn episodes. To quantify the contribution of biomass burning to SOC, the observed VOCs
537 were apportioned to different sources, including biomass burning with CH_3CN as the tracer. The
538 source profiles are provided in Figure S12 in the Supplementary Material. According to the
539 SVOCs simulated on the basis of VOCs emitted from biomass burning, the SVOCs were
540 elevated by $15.4\% \pm 1.3\%$ due to biomass burning during the episodes.

541 In contrast, the correlations were much worse in summer ($R^2 = 0.01$ and 0.31 for daily and
542 diurnal variations, respectively). The high frequency (50.8%) of rainy days in summer was a
543 factor for the poor correlation; for example, the level of SOC was low during the late period of
544 June when the precipitation lasted for about 10 days, and the model overestimated the SVOCs
545 without considering the influence of precipitation. The correlations between SOC and SVOCs
546 ($R^2 = 0.14$ and 0.19 for the daily and diurnal variations, respectively) were still poor even after
547 the rainy days were excluded. Hence, the poor correlation should also be related to other factors,
548 such as incomplete consideration of the contribution of biogenic VOCs. Although isoprene was
549 included as a precursor of the SVOCs, other biogenic species (i.e., α -pinene, β -pinene, and

550 monoterpenes) that were proven to be important precursors of SOC (Kanakidou et al., 2005)
 551 were not monitored in this study. Moreover, the level of biogenic VOCs was much higher in
 552 summer than in autumn. Taking isoprene as an example, the mixing ratio of isoprene was $66.7 \pm$
 553 4.9 pptv in summer and only 37.2 ± 2.6 pptv in autumn. The higher missing level of biogenic
 554 VOCs in summer led to a higher deficit of SVOCs, perhaps causing the poorer correlation
 555 between SOC and SVOCs. Nevertheless, this notion needs requires validation with more
 556 comprehensive data on biogenic VOCs.

557



558
 559 **Figure 14. Correlations between calculated SOC and simulated SVOCs in (a) day-to-day**
 560 **variation and (b) diurnal pattern.**

561

562 4. Conclusions

563 In summer and autumn 2014, the concentrations of $PM_{2.5}$ and its components were continuously
 564 monitored in Wuhan; six $PM_{2.5}$ episodes were captured. The analysis of $PM_{2.5}$ concentrations and
 565 compositions found that Wuhan suffered from relatively high levels of $PM_{2.5}$, even in the warm
 566 seasons. Secondary inorganic ions were the most predominant species in $PM_{2.5}$ in the form of
 567 NH_4NO_3 and $(NH_4)_2SO_4$. Comparable levels of SO_4^{2-} and NO_3^- indicate that stationary and
 568 mobile sources had equivalent importance in Wuhan. With the EC-tracer method, it was found
 569 that the POC level was slightly higher than that of SOC, and both increased significantly during
 570 the episodes. K was the most abundant element in $PM_{2.5}$, implying biomass burning in and

571 around Wuhan during the sampling campaign. **Indeed, the source apportionment revealed that**
572 **biomass burning was the main cause of increases in PM_{2.5} in episodes 1, 3, and 4. Fugitive dust**
573 **was the leading factor in episode 2. However, episodes 5 and 6 were mainly attributable to**
574 **vehicle emissions and SIAs.** Study of the formation mechanism of NO₃⁻ and SOC found that
575 NO₃⁻ was mainly generated from the homogeneous reactions in episode 6, and the high levels of
576 NO_x and NH₃ and the low temperature caused the increase in NO₃⁻. Furthermore, the daily and
577 diurnal variations of SOC correlated well with those of SVOCs in autumn. Aromatics and
578 isoprene were the main precursors of SOC, and the contribution of aromatics increased during
579 the episodes. However, the correlation between SOC and SVOCs was much worse in summer,
580 possibly as a result of the incompleteness of the biogenic VOC input in the simulation of SVOCs.
581 This study **advances our understanding of the** chemical characteristics of PM_{2.5} in warm seasons
582 in Wuhan and for the first time quantifies the contribution of biomass burning to PM_{2.5}. The
583 investigation of SOC formation will also inspire the application of the explicit chemical
584 mechanisms on the study of SOA.

585
586 **Acknowledgments:** This study was supported by the Research Grants Council of the Hong
587 Kong Special Administrative Region via grants PolyU5154/13E, PolyU152052/14E,
588 CRF/C5022-14G, and CRF/C5504-15E and the Hong Kong Polytechnic University PhD
589 scholarships (project #RTUP). This study is partly supported by the Hong Kong PolyU internal
590 grant (1-ZVCX and 4-BCAV) and the National Natural Science Foundation of China (No.
591 41275122).

593 **References**

- 594 Anderson, J.O., Thundiyil, J.G., and Stolbach, A., 2012: Clearing the air: A review of the effects
595 of particulate matter air pollution on human health. *J. Med. Toxicol.* 8, 166-175.
- 596 Aumont, B., Madronich, S., Ammann, M., Kalberer, M., Baltnesperger, U., Hauglustaine, D., and
597 Baltnesperger, F., 1999: On the NO₂ + soot reaction in the atmosphere. *J. Geophys. Res.* 104,
598 1729-1736.
- 599 Barwise, A.J.G., 1990: Role of nickel and vanadium in petroleum classification. *Energy & Fuels*
600 4, 647-652.
- 601 Brown, S.G., Frankel, A., and Hafner, H.R., 2007: Source apportionment of VOCs in Los

602 Angeles area using positive matrix factorization. *Atmos. Environ.* 41, 227-237.

603 Cabada, J.C., Pandis, S.N., Subramanian, R., Robinson, A.L., Polidori, A., and Turpin, B., 2004:
604 Estimating the secondary organic aerosol contribution to PM_{2.5} using the EC tracer method.
605 *Aerosol Sci. Tech.* 38, 140-155.

606 Cao, J.J., Shen, Z.X., Chow, J.C., Watson, J.G., Lee, S.C., Tie, X.X., Ho, K.F., Wang, G.H., and
607 Han, Y.M., 2012: Winter and summer PM_{2.5} chemical compositions in fourteen Chinese cities.
608 *J. Air Waste Manage. Assoc.* 62, 1214-1226.

609 Cao, J.J., Wu, F., Chow, J.C., Lee, S.C., Li, Y., Chen, S.W., An, Z.S., Fung, K.K., Watson, J.G.,
610 Zhu, C.S., and Liu, S.X., 2005: Characterization and source apportionment of atmospheric
611 organic and elemental carbon during fall and winter of 2003 in Xi'an, China. *Atmos. Chem.*
612 *Phys.* 5, 3127-3137.

613 Cheng, H.R., Gong, W., Wang, Z.W., Zhang, F., Wang, X.M., Lv, X.P., Liu, J., Fu, X.X., and
614 Zhang, G., 2014: Ionic composition of submicron particles (PM_{1.0}) during the long-lasting
615 haze period in January 2013 in Wuhan, central China. *J. Environ. Sci.* 26(4), 810-817.

616 Cheng, H.R., Guo, H., Wang, X.M., Saunders, S.M., Lam, S.H.M., Jiang, F., Wang, T.J., Ding,
617 A.J., Lee, S.C., and Ho, K.F., 2010: On the relationship between ozone and its precursors in
618 the Pearl River Delta: application of an observation-based model (OBM). *Environ. Sci. Pollut.*
619 *Res.* 17, 547-560.

620 Chow, J.C., Watson, J.G., Lu, Z.Q., Lowenthal, D.H., Frazier, C.A., Solomon, P.A., Thuillier,
621 R.H., and Magliano, K., 1996: Descriptive analysis of PM_{2.5} and PM₁₀ at regionally
622 representative locations during SJVAQS/AUSPEX. *Atmos. Environ.* 30(12), 2079-2112.

623 de Fatima Andrade, M., de Miranda, R.M., Fornaro, A., Kerr, A., Oyama, B., de Andre, P.A., and
624 Saldiva, P., 2012. Vehicle emissions and PM_{2.5} mass concentrations in six Brazilian cities. *Air*
625 *Qual. Atmos. Health* 5(1), 79-88.

626 Deng, X.J., Li, F., Li, Y.H., Li, J.Y., Huang, H.Z., and Liu, X.T., 2015: Vertical distribution
627 characteristics of PM in the surface layer of Guangzhou. *Particuology* 20, 3-9.

628 Deng, X.J., Tie, X.X., Zhou, X.J., Wu, D., Zhong, L.J., Tan, H.B., Li, F., Huang, X.Y., Bi, X.Y.,
629 and Deng, T., 2008: Effects of Southeast Asia biomass burning on aerosols and ozone
630 concentrations over the Pearl River Delta (PRD) region. *Atmos. Environ.* 43(36), 8493-8501.

631 Duan, F.K., He, K.B., Ma, Y.L., Jia, Y.T., Yang, F.M., Lei, Y., Tanaka, S., and Okuta, T., 2005:
632 Characteristics of carbonaceous aerosols in Beijing, China. *Chemosphere* 60(3), 355-364.

633 Echalar, F., Gaudichet, A., Cachier, H., and Artaxo, P., 1995: Aerosol emissions by tropical forest
634 and savanna biomass burning: characteristic trace elements and fluxes. *Geophys. Res. Lett.* 22,
635 3039-3042.

636 Emmerson, K.M., Carslaw, N., Carpenter, L.J., Heard, D.E., Lee, J.D., and Pilling, M.J., 2005.
637 *Urban atmospheric chemistry during the PUMA campaign 1: Comparison of modelled OH and*
638 *HO₂ concentrations with measurements. J. Atmos. Chem.* 52, 143-164.

639 Forstner, H.J.L., Flagan, R.C., and Seinfeld, J.H., 1997: Secondary organic aerosol from the
640 photooxidation of aromatic hydrocarbons: molecular composition. *Environ. Sci. Technol.* 31
641 (5), 1345-1358.

642 Friedli, H.R., Radke, L.F., Lu, J.Y., Banic, C.M., Leaitch, W.R., and MacPherson, J.I., 2003:
643 Mercury emissions from burning of biomass from temperate North American forests:
644 laboratory and airborne measurements. *Atmos. Environ.* 37, 253-267.

645 GB 3095-2012, accessible from [http://kjs.mep.gov.cn/hjbhbz/bzwb/dqhjbh/dqhjzlbz/201203/](http://kjs.mep.gov.cn/hjbhbz/bzwb/dqhjbh/dqhjzlbz/201203/W020120410330232398521.pdf)
646 [W020120410330232398521.pdf](http://kjs.mep.gov.cn/hjbhbz/bzwb/dqhjbh/dqhjzlbz/201203/W020120410330232398521.pdf).

647 Geng, F.H., Zhang, Q., Tie, X.X., Huang, M.Y., Ma, X.C., Deng, Z.Z., Yu, Q., Quan, J.N., and
648 Zhao, C.S., 2009: Aircraft measurements of O₃, NO_x, CO, VOCs, and SO₂ in the Yangtze
649 River Delta region. *Atmos. Environ.* 43, 584-593.

650 Goldberg, M.S., Burnett, R.T., Bailar III, J.C., Brook, J., Bonvalot, Y., Tamblyn, R., Singh, R.,
651 and Valois, M.F., 2001: The association between daily mortality and ambient air particle
652 pollution in Montreal, Quebec: 1. Nonaccidental mortality. *Environ. Res.* 86(1), 12-25.

653 Gugamsetty, B., Wei, H., Liu, C.N., Awasthi, A., Hsu, S.C., Tsai, C.J., Roan, G.D., Wu, Y.C., and
654 Chen, C.F., 2012: Source Characterization and Apportionment of PM₁₀, PM_{2.5} and PM_{0.1} by
655 Using Positive Matrix Factorization. *Aerosol Air Qual. Res.* 12, 476-491.

656 Guo, H., Cheng, H.R., Ling, Z.H., Louie, P.K.K., and Ayoko, G.A., 2011b: Which emission
657 sources are responsible for the volatile organic compounds in the atmosphere of Pearl River
658 Delta? *J. Hazard. Mater.* 188, 116-124.

659 Guo, H., Zou, S.C., Tsai, W.Y., Chan, L.Y., and Blake, D.R., 2011a: Emission characteristics of
660 nonmethane hydrocarbons from private cars and taxis at different driving speeds in Hong
661 Kong. *Atmos. Environ.* 45, 2711-2721.

662 Ho, K.F., Lee, S.C., Chan, C.K., Yu, J.C., Chow, J.C., and Yao, X.H., 2003: Characterization of
663 chemical species in PM_{2.5} and PM₁₀ aerosols in Hong Kong. *Atmos. Environ.* 37(1), 31-39.

664 HKEPD, 2014. Air Quality in Hong Kong 2014, accessible at
665 <http://www.aqhi.gov.hk/en/download/air-quality-reportse469.html?showall=&start=1>.

666 Hu, J.H., and Abbatt, J.P.D., 1997: Reaction probabilities for N₂O₅ hydrolysis on sulfur acid and
667 ammonium sulfate aerosols at room temperature. *J. Phys. Chem.* 101A, 871-878.

668 Kanakidou, M., Seinfeld, J.H., Pandis, S.N., Barnes, I., Dentener, F.J., Facchini, M.C., Dingenen,
669 R.V., Ervens, B., Nenes, A., Nielsen, C.J., Swietlicki, E., Putaud, J.P., Balkanski, Y., Fuzzi, S.,
670 Horth, J., Moortgat, G.K., Winterhalter, R., Myhre, C.E.L., Tsigaridis, K., Vignati, E.,
671 Stephanou, E.G., and Wilson, J., 2005: Organic aerosol and global climate modelling: a review.
672 *Atmos. Chem. Phys.* 5, 1053-1123.

673 Kanaya, Y., Sadanaga, Y., Matsumoto, J., Sharma, U.K., Hirokawa, J., Kajii, Y., and Akimoto, H.,
674 1999: Nighttime observation of the HO₂ radical by an LIF instrument at Oki Island, Japan, and
675 its possible origins. *Geophys. Res. Lett.* 26, 2179-2182.

676 Kang, H.Q., Zhu, B., Su, J.F., Wang, H.L., Zhang, Q.C., and Wang, F., 2013: Analysis of a long-
677 lasting haze episode in Nanjing, China. *Atmos. Res.* 120-121, 78-87.

678 Kerminen, V.M., Hillamo, R., Teinila, K., Pakkanen, T., Allegrini, I., and Sparapani, R., 2001:
679 Ion balances of size-resolved tropospheric aerosol samples: implications for the acidity and
680 atmospheric processing of aerosols. *Atmos. Environ.* 35(31), 5255-5265.

681 Koe, L.C.C., Jr, A.F.A., and McGregor, J.L., 2001: Investigating the haze transport from 1997
682 biomass burning in Southeast Asia: its impact upon Singapore. *Atmos. Environ.* 35(15), 2723-
683 2734.

684 Lam, S.H.M., Saunders, S.M., Guo, H., Ling, Z.H., Jiang, F., Wang, X.M., and Wang, T.J., 2013:
685 Modelling VOC source impacts on high ozone episode days observed at a mountain summit in
686 Hong Kong under the influence of mountain-valley breezes. *Atmos. Environ.* 81, 166-176.

687 Lee, E., Chan, C.K., and Paatero, P., 1999: Application of positive matrix factorization in source
688 apportionment of particulate pollutants in Hong Kong. *Atmos. Environ.* 33, 3201-3212.

689 Lin, Y.C., Cheng, M.T., Lin, W.H., Lan, Y.Y., and Tsuang, B.J., 2010: Causes of the elevated
690 nitrated aerosol levels during episodic days in Taichung urban area, Taiwan. *Atmos. Environ.*
691 44, 1632-1640.

692 Ling, Z.H., Guo, H., Lam, S.H.M., Saunders, S.M., and Wang, T., 2014: Atmospheric
693 photochemical reactivity and ozone production at two sites in Hong Kong: Application of a
694 master chemical mechanism-photochemical box model. *J. Geophys. Res. Atmos.* 119, 10567-

695 10582.

696 Liu, Y.J., Zhang, T.T., Liu, Q.Y., Zhang, R.J., Sun, Z.Q., and Zhang, M.G., 2014: Seasonal
697 variation of physical and chemical properties in TSP, PM₁₀ and PM_{2.5} at a roadside site in
698 Beijing and their influence on atmospheric visibility. *Aerosol Air Qual. Res.* 14, 954-969.

699 Liu, Z.R., Hu, B., Wang, L.L., Wu, F.K., Gao, W.K., and Wang, Y.S., 2015: Seasonal and diurnal
700 variation in particulate matter (PM₁₀ and PM_{2.5}) at an urban site of Beijing: analyses from a 9-
701 year study. *Environ. Sci. Pollut. Res.* 22, 627-642.

702 Lyu, X.P., Chen, N., Guo, H., Zhang, W.H., Wang, N., Wang, Y., and Liu, M., 2016: Ambient
703 volatile organic compounds and their effect on ozone production in Wuhan, central China. *Sci.*
704 *Total Environ.* 541, 200-209.

705 Lyu, X.P., Ling, Z.H., Guo, H., Saunders, S.M., Lam, S.H.M., Wang, N., Wang, Y., Liu, M., and
706 Wang, T., 2015 (b): Re-examination of C₁-C₅ alkyl nitrates in Hong Kong using an
707 observation-based model. *Atmos. Environ.* 120, 28-37.

708 Lyu, X.P., Wang, Z.W., Cheng, H.R., Zhang, F., Zhang, G., Wang, X.M., Ling, Z.H., Wang, N.,
709 2015 (a): Chemical characteristics of submicron particulates (PM_{1.0}) in Wuhan, Central China.
710 *Atmos. Res.* 161-162, 169-178.

711 Nemesure, S., Wagener, R., and Schwartz, S.E., 1995: Direct shortwave forcing of climate by the
712 anthropogenic sulfate aerosol: sensitivity to particle size, composition, and relative humidity. *J.*
713 *Geophys. Res.* 100, 26105-26116.

714 Nriagu, J.O., and Pacyna, J.M., 1988: Quantitative assessment of worldwide contamination of air,
715 water and soils by trace metals. *Nature* 333, 134-139.

716 Oanh, N.T.K., and Leelasakultum, K., 2011: Analysis of meteorology and emission in haze
717 episode prevalence over mountain-bounded region for early warning. *Sci. Total Environ.*
718 409(11), 2261-2271.

719 Paatero, P., and Tapper, U., 1994: Positive matrix factorization: A non-negative factor model with
720 optimal utilization of error estimates of data values. *Environmetrics* 5, 111-126.

721 Paatero, P., 1997: Least squares formulation of robust non-negative factor analysis. *Chemom.*
722 *Intell. Lab. Sys.* 37, 23-35.

723 Pathak, R.K., Wang, T., and Wu, W.S., 2011: Nighttime enhancement of PM_{2.5} nitrate in
724 ammonia-poor atmospheric conditions in Beijing and Shanghai: Plausible contributions of
725 heterogeneous hydrolysis of N₂O₅ and HNO₃ partitioning. *Atmos. Environ.* 45, 1183-1191.

726 Querol, X., Alastuey, A., Viana, M.M., Rodriguez, S., Artinano, B., Salvador, P., Garcia do
727 Santos, S., Fernandez Patier, R., Ruiz, C.R., de la Rosa, J., Sanchez de la Campa, A.,
728 Menendez, M., and Gil, J.I., 2004: Speciation and origin of PM₁₀ and PM_{2.5} in Spain. *J.*
729 *Aerosol Sci.* 35, 1151-1172.

730 Ramanathan, V., Crutzen, P.J., Kiehl, J.T., and Rosenfeld, D., 2001: Aerosol, climate and the
731 hydrological cycle. *Science* 294, 2119-2124.

732 Saarikoski, S., Sillanpaa, M., Sofiev, M., Timonen, H., Saarnio, K., Teinila, K., Karppinen, A.,
733 Kukkonen, J., and Hillamo, R., 2007: Chemical composition of aerosols during a major
734 biomass burning episode over northern Europe in spring 2006: Experimental and modelling
735 assessments. *Atmos. Environ.* 41, 3577-3589.

736 Seinfeld, J.H., and Pandis, S.N., 1998: Atmospheric chemistry and physics from air pollution to
737 climate change. New York: Wiley, p. 528.

738 Shen, G.F., Yuan, S.Y., Xie, Y.N., Xia, S.J., Li, L., Yao, Y.K., Qiao, Y.Z., Zhang, J., Zhao, Q.Y.,
739 Ding, A.J., Li, B., and Wu, H.S., 2014: Ambient levels and temporal variations of PM_{2.5} and
740 PM₁₀ at a residential site in the mega-city, Nanjing, in the western Yangtze River Delta, China.
741 *J. Environ. Sci. Health: Part A* 49(2), 171-178.

742 Shen, Z.X., Cao, J.J., Liu, S.X., Zhu, C.S., Wang, X., Zhang, T., Xu, H.M., and Hu, T.F., 2011:
743 Chemical compositions of PM₁₀ and PM_{2.5} collected at ground level and 100 meters during a
744 strong winter-time pollution episode in Xi'an, China. *J Air Waste Manage. Assoc.* 61(11),
745 1150-1159.

746 Simoneit, B.R.T., 2002: Biomass burning-a review of organic tracers for smoke from incomplete
747 combustion. *Appl. Geochem.* 17(3), 129-162.

748 Song, S., Wu, Y., Jiang, J., Yang, L., Cheng, Y., and Hao, J., 2012. Chemical characteristics of
749 size-resolved PM_{2.5} at a roadside environment in Beijing, China. *Environ. Pollut.* 161, 215-221.

750 Takekawa, H., Minoura, H., and Yamazaki, S., 2003. Temperature dependence of secondary
751 organic aerosol formation by photo-oxidation of hydrocarbons. *Atmos. Environ.* 37, 3413-
752 3424.

753 Tang, I.N., and Munkelwitz, H.R., 1993: Compositions and temperature dependence of the
754 deliquescence properties of hygroscopic aerosols. *Atmos. Environ.* 27, 467-473.

755 Theodosi, C., Grivas, G., Zarnpas, P., Chaloulakou, A., and Mihalopoulos, N., 2011: Mass and
756 chemical composition of size-segregated aerosols (PM₁, PM_{2.5}, PM₁₀) over Athens, Greece:

757 local versus regional sources. *Atmos. Chem. Phys.* 11, 11895-1191.

758 Wang, H., Tan, S.C., Wang, Y., Jiang, C., Shi, G.Y., Zhang, M.X., and Che, H.Z., 2014 (a): A
759 multisource observation study of the severe prolonged regional haze episode over eastern
760 China in January 2013. *Atmos. Environ.* 89, 807-815.

761 Wang, H., Xu, J.Y., Zhang, M., Yang, Y.Q., Shen, X.J., Wang, Y.Q., Chen, D., and Guo, J.P., 2014
762 (b): A study of the meteorological causes of a prolonged and severe haze episode in January
763 2013 over central-eastern China. *Atmos. Environ.* 98, 146-157.

764 Wang, H.L., Lou, S.R., Huang, C., Qiao, L.P., Tang, X.B., Chen, C.H., Zeng, L.M., Wang, Q.,
765 Zhou, M., Lu, S.H., and Yu, X.N., 2014: Source profiles of volatile organic compounds from
766 biomass burning in Yangtze River Delta, China. *Aerosol Air Qual. Res.* 14, 818-828.

767 Wang, J., Hu, Z.M., Chen, Y.Y., Chen, Z.L., and Xu, S.Y., 2013: Contamination characteristics
768 and possible sources of PM₁₀ and PM_{2.5} in different functional areas of Shanghai, China.
769 *Atmos. Environ.* 68, 221-229.

770 Wang, P., Cao, J.J., Tie, X.X., Wang, G.H., Li, G.H., Hu, T.F., Wu, Y.T., Xu, Y.S., Xu, G.D., Zhao,
771 Y.Z., Ding, W.C., Liu, H.K., Huang, R.J., and Zhan, C.L., 2015: Impact of meteorological
772 parameters and gaseous pollutants on PM_{2.5} and PM₁₀ mass concentrations during 2010 in
773 Xi'an, China. *Aerosol Air Qual. Res.* 15, 1844-1854.

774 Wang, S.X., Zhang, L., Li, G.H., Wu, Y., Hao, J.M., Pirrone, N., Sprovieri, F., and Ancora, M.P.,
775 2010. Mercury emission and speciation of coal-fired power plants in China. *Atmos. Chem.*
776 *Phys.* 10, 1183-1192.

777 Wang, Y.X., Zhang, Q.Q., Jiang, J.K., Zhou, W., Wang, B.Y., He, K.B., Duan, F.K., Zhang, Q.,
778 Philip, S., and Xie, Y.Y., 2014: Enhanced sulfate formation during China's severe winter haze
779 episode in January 2013 missing from current models. *J. Geophys. Res.* 119, 10425-10440.

780 White, W.H., and Roberts, P.T., 1977: On the nature and origins of visibility-reducing aerosols in
781 the Los Angeles air basin. *Atmos. Environ.* 11(9), 803-812.

782 Wuhan Environmental Bulletin, 2014, accessible at [http://www.whepb.gov.cn/zwGkhjtj/
783 16240.jhtml](http://www.whepb.gov.cn/zwGkhjtj/16240.jhtml).

784 Yang, L., Cheng, S., Wang, X., Nie, W., Xu, P., Gao, X., Yuan, C., and Wang, W., 2013. Source
785 identification and health impact of PM_{2.5} in a heavily polluted urban atmosphere in China.
786 *Atmos. Environ.* 75, 265-269.

787 Yang, L.X., Zhou, X.H., Wang, Z., Zhou, Y., Cheng, S.H., Xu, P.J., Gao, X.M., Nie, W., Wang,

788 X.F., and Wang, W.X., 2012: Airborne fine particulate pollution in Jinan, China:
789 Concentrations, chemical compositions and influence on visibility impairment. *Atmos.*
790 *Environ.* 55, 506-514.

791 Yao, X.H., Chan, C.K., Fang, M., Candle, S., Chan, T., Mulawa, P., He, K.B., and Ye, B., 2002:
792 The water-soluble ionic composition of PM_{2.5} in Shanghai and Beijing, China. *Atmos. Environ.*
793 36(26), 4223-4234.

794 Ye, B., Ji, X., Yang, H., Yao, X., Chan, C.K., Cadle, S.H., Chan, T., and Mulawa, P.A., 2003.
795 Concentration and chemical composition of PM_{2.5} in Shanghai for a 1-year period. *Atmos.*
796 *Environ.* 37, 499-510.

797 Zhang, F., Cheng, H.R., Wang, Z.W., Lv, X.P., Zhu, Z.M., Zhang, G., and Wang, X.M., 2014:
798 Fine particles (PM_{2.5}) at a CAWNET background site in Central China: Chemical
799 compositions, seasonal variations and regional pollution events. *Atmos. Environ.* 86, 193-202.

800 Zhang, G.H., Bi, X.H., Chan, L.Y., Wang, X.M., Sheng, G.Y., and Fu, J.M., 2013: Size-
801 segregated chemical characteristics of aerosol during haze in an urban area of the Pearl River
802 Delta region, China. *Urban Climate* 4, 74-84.

803 Zhang, Q., Jimenez, J.L., Worsnop, D.R., Canagaratna, M., 2007: A case study of urban particle
804 acidity and its influence on secondary organic aerosol. *Environ. Sci. Technol.* 41(9), 3213-
805 3219.

806 Zhang, X.Y., Wang, Y.Q., Niu, T., Zhang, X.C., Gong, S.L., Zhang, Y.M., and Sun, J.Y., 2012:
807 Atmospheric aerosol compositions in China: Spatial/temporal variability, chemical signature,
808 regional haze distribution and comparisons with global aerosols. *Atmos. Chem. Phys.* 12, 779-
809 799.

810 Zhang, Y.Y., Obrist, D., Zielinska, B., and Gertler, A., 2013: Particulate emissions from different
811 types of biomass burning. *Atmos. Environ.* 72, 27-35.

812 Zheng, M., Salmon, L.G., Schauer, J.J., Zeng, L.M., Kiang, C.S., Zhang, Y.H., and Cass, G.R.,
813 2005: Seasonal trends in PM_{2.5} source contributions in Beijing, China. *Atmos. Environ.* 39(22),
814 3967-3976.